DEVELOPMENT OF IN SITU 3D BIOPRINTING STRATEGY FOR THE REGENERATION OF CRANIOFACIAL BONE

A THESIS SUBMITTED TO
THE GRADUATE SCHOOL OF NATURAL AND APPLIED SCIENCES
OF
ANKARA UNIVERSITY

by

Osama HINDI

IN PARTIAL FULFILLMENT OF THE REQUIREMENTS
FOR THE DEGREE OF
MASTER OF SCIENCE
IN
BIOMEDICAL ENGINEERING

ANKARA
2024

ABSTRACT

MSc Thesis

DEVELOPMENT OF IN SITU 3D BIOPRINTING STRATEGY FOR THE REGENERATION OF CRANIOFACIAL BONE

Osama HINDI

Ankara University
Graduate School of Natural and Applied Sciences
Department of Biomedical Engineering

Supervisor: Prof. Dr. Pınar YILGÖR HURİ
Co-Supervisor: Prof. Dr. Çağdaş OTO

The advancement of three-dimensional (3D) bioprinting has indicated a significant transformation in tissue engineering and regenerative medicine. This thesis investigates the feasibility and effectiveness of *in situ* 3D bioprinting for craniofacial bone regeneration. Traditional methods for treating bone defects often face challenges such as donor availability, multiple surgeries, and limited osteogenic properties. In contrast, 3D bioprinting offers a promising alternative by precisely depositing cells and biomaterials to create tissue scaffolds that match the damaged area's shape and properties. The primary objective of this research is to develop a clinically translatable *in situ* 3D bioprinting strategy for bone regeneration. The approach involves using computer-aided design (CAD) and computer-aided manufacturing (CAM) toolkit to model and 3D print scaffolds directly onto damaged tissues. This method eliminates the time-consuming and costly two-step process of in vitro and in vivo experimentation. A key novelty of this study is the application of the *in situ* bioprinting technique directly onto the whole bodies of live animals, which differentiates it from current works that often rely on ex vivo or isolated tissue models. This live-animal approach ensures a more accurate representation of clinical conditions and challenges, enhancing the potential for clinical translation. Preclinical studies were conducted using a rabbit model to validate the effectiveness of the proposed *in situ* bioprinting technique. Critical-sized bone defects were created on the parietal bones of the rabbits, followed by the application of an adipose-derived stem cell laden alginate/hydroxyapatite bioink using a 3D bioprinter. Post-operative evaluations included Computed Tomography (CT) scans, histopathological analysis and micro-CT to assess bone healing and bone-material integration. The results demonstrated successful bone regeneration with the *in situ* bioprinting approach, indicating its potential for clinical applications. This method provides a rapid, patient-specific, and effective regenerative therapy by directly applying necessary biophysical and biochemical stimuli to the damaged area. In conclusion, this thesis contributes to the growing body of evidence supporting *in situ* 3D bioprinting as a viable and promising technique for craniofacial bone regeneration, with potential implications for broader clinical applications in tissue engineering and regenerative medicine.

August 2024, 80 pages

Key Words: In situ bioprinting; Craniofacial bone regeneration; 3D bioprinting; Tissue engineering; Regenerative medicine

ÖZET

Yüksek Lisans Tezi

KRANİYOFASİYAL KEMİĞİN REJENERASYONU İÇİN *in situ* 3B BİYOBASKI STRATEJİSİNİN GELİŞTİRİLMESİ

Osama HINDI

Ankara Üniversitesi
Fen Bilimleri Enstitüsü
Biyomedikal Mühendisliği Anabilim Dalı

Danışman: Prof. Dr. Pınar YILGÖR HURİ
Eş Danışman: Prof. Dr. Çağdaş OTO

Bu tez çalışmasında *in situ* 3B biyobaskı yaklaşımının kraniofasiyal kemik rejenerasyonu için uygulanabilirli ve etkinliği araştırılmıştır. Kemik defektlerini tedavi etmek için kullanılan geleneksel yöntemler, genellikle donör bulunabilirliği, çoklu ameliyatlar ve sınırlı osteojenik özellikler gibi zorluklarla karşı karşıya kalmaktadır. Buna karşın, 3B biyobaskı, hücreleri ve biyomalzemelerin hassas konumlanmasını kontrol ederek hasar görmüş bölgenin şekline ve özelliklerine uygun doku iskeleleri oluşturma imkanı sağlamaktadır. Bu araştırmanın birincil amacı, kemik rejenerasyonu için klinik olarak uygulanabilir bir *in situ* 3B biyobaskı stratejisi geliştirmektir. Bu yaklaşım, defekt bölgesine doğrudan modelleme ve baskı yapma işlemini gerçekleştirmek için bilgisayar destekli tasarım (CAD) ve bilgisayar destekli üretim (CAM) yaklaşımlarının kullanılmasını içermektedir. Bu çalışmanın temel yeniliği, *in situ* biyobaskı tekniğinin canlı hayvanların tüm vücutlarına doğrudan uygulanmasıdır ki bu, mevcut çalışmaların genellikle ex vivo veya izole doku modellerine dayandığı bir yaklaşımdan ayrılmaktadır. Canlı hayvan yaklaşımı, klinik koşulların ve zorlukların daHAp doğru bir şekilde temsil edilmesini sağlayarak klinik uygulama potansiyelini artırmaktadır. Preklinik çalışmalar, önerilen *in situ* biyobaskı tekniğinin etkinliğini doğrulamak amacıyla bir tavşan modelinde gerçekleştirilmiştir. Tavşanların parietal kemiklerinde kritik boyutlu kemik defektleri oluşturulmuş ve ardından bir 3B biyoyazıcı kullanılarak aljinat ve kalsiyum fosfat içerikli ve tavşan yağ kaynaklı mezenkimal kök hücre içeren biyomürekkep uygulanmıştır. Post-operatif değerlendirmeler arasında BT taramaları, histopatolojik analizler, mikro-CT ve mekanik testler gerçekleştirilerek, kemik rejenerasyonu ve doku-malzeme entegrasyonu değerlendirilmiştir. Sonuçlar, *in situ* biyobaskı yaklaşımı ile başarılı kemik rejenerasyonunu göstermiş ve bu yöntemin klinik uygulamalar için potansiyelini ortaya koymuştur. Bu yöntem, gerekli biyofiziksel ve biyokimyasal uyarıları doğrudan hasar görmüş alana uygulayarak hızlı, hasta-spesifik ve etkili bir rejeneratif terapi sunmaktadır. Sonuç olarak, bu tez, *in situ* 3B biyobaskının kraniofasiyal kemik rejenerasyonu için uygulanabilir ve umut verici bir teknik olduğunu, ve doku mühendisliği ve rejeneratif tıptaki daHAp geniş klinik uygulamalar için potansiyel etkilerini vurgulamaktadır.

Ağustos 2024, 80 sayfa

Anahtar Kelimeler: In situ biyobaskı; Kraniyofasiyal kemik rejenerasyonu; 3D biyobaskı; Doku mühendisliği; Rejeneratif tıp

FOREWORD AND ACKNOWLEDGEMENTS

I would like to extend my deepest gratitude to my supervisor, Prof. Dr. Pınar Yilgör Huri, for her invaluable guidance, support, and encouragement throughout my thesis journey. I am truly grateful for the time and knowledge she has generously shared during my graduate years. Her expertise and patience have greatly enhanced both my thesis and my overall scientific understanding.

I am also deeply appreciative of my co-supervisor Prof. Dr. Çağdaş Oto for his unwavering support and for providing me with the opportunity to expand my scientific knowledge. His contributions have been vital to the success of this research, and I am fortunate to have had the chance to work closely with him. I would also like to express my sincere gratitude to his team, including Research Assistants Dr. Merve Bakıcı, Dr. Burçin Demirtaş, Barış Batur, Orçun Güvener, and student Gülezgi Karadağ, for their assistance and collaboration throughout this project.

A special mention to Dr. Arda Büyüksungur, whose constructive feedback and support in the CT scans and data analysis provided invaluable assistance during my research. His insights and dedication made a significant difference in the progress and completion of my work.

Special thanks are due to all MTE Lab members for creating a collaborative and enriching environment and helped me successfully complete this study especially Dr. Emre Ergene and Şeyda Gökyer. I am also very grateful to my other lab colleagues Işıl Yazgan, Utku Serhat Derici, Barış Burak Altunay, Begüm Pınarbaşı, and Ayşe Yalçiner for their assistance, their kind friendship and for their suggestions and help throughout this thesis.

I would like to acknowledge the financial support provided by TÜBİTAK; Center of Excellence Support Program (1004 Program) through project 22AG055, without which this research would not have been possible. The resources provided have been crucial to the successful completion of this work.

I wish to express my sincere gratitude to Prof. Dr. Oğuzhan Gündüz and his team — Eray Altan, Esra Pılavcı, and Dilruba Baykara — at the Center for Nanotechnology & Biomaterials Research at Marmara University. The opportunity to work in his lab for an extended period before starting my master's studies significantly influenced the direction of my research and profoundly enhanced both my thesis and my overall scientific understanding.

Special thanks to my brother, Bilal Hindi, for his unwavering support in every possible way. His encouragement, care, and belief in me have been a constant source of strength throughout this journey.

Additionally, I am very grateful to my close friends Dr. Marwan Hammami and Mehmet Ali. Your friendship and support have been a source of great strength and inspiration, and I deeply appreciate your presence and support during my hard times.

Moreover, I would like to extend my deepest gratitude to the people of my homeland, Palestine. Their courage and resilience during challenging times have been a powerful source of inspiration. My heartfelt appreciation goes out to my great friends who have

martyred and whom I have lost in recent months due to the ongoing conflict. Their memory and sacrifice will forever remain a guiding light and be remembered with honor.

I would like to thank my entire family for their support and encouragement, which have provided me with the strength I needed throughout this journey.

I also would like to express my heartfelt thanks to my dear parents, Najat Dabdoub and Ali Hindi for their love, care, and support. Their belief in me has been a guiding force, and I am sincerely grateful for their presence in my life.

For all the people who contributed in many other ways I am forever grateful.

May God bless all of you.

Osama HINDI
Ankara, August 2024

TABLE OF CONTENTS

SYMBOLS AND ABBREVIATIONS

3D	Three-Dimensional
2D	Two-Dimensional
ALG	Alginate
AM	Additive manufacturing
ANOVA	Analysis of variance
ASCs	Adipose-derived stem cells
bFGF	Fibroblast growth factor
BMD	Bone Mineral Density
BMPs	Bone morphogenetic proteins
BSA	Bovine serum albumin
Ca^{2+}	Calcium
$CaCl_2$	Calcium chloride
CAD	Computer-aided design
CAM	Computer-aided manufacturing
CT	Computed Tomography
DMEM	Dulbecco's Modified Eagle Medium
DMSO	Dimethyl Sulfoxide
ECM	Extracellular matrix
EDTA	Ethylenediaminetetraacetic Acid
F/S	Fail/Success
FBS	Fetal bovine serum
FDM	Fused deposition modeling
GelMA	Gelatin Methacrylate
HA	Hyaluronic acid
HAMA	Modified hyaluronic acid
HAp	Hydroxyapatite
MPa	Megapascal
MRI	Magnetic resonance imaging
n-HA	Nano-hydroxyapatite
OCT	Optical coherence tomography

OH^-	Hydroxide
P/S	Penicillin/streptomycin
PBS	Phosphate-buffered saline
PCL	Polycaprolactone
PEG	Polyethylene glycol
PGA	Poly(glycolic acid)
PLA	Poly(lactic acid)
PLGA	Poly(lactic-co-glycolic acid)
PO_4^{3-}	Phosphate
ROI	Region of interest
RT	Room temperature
SD	Standard deviation
SEM	Scanning Electron Microscopy
SLA	Stereolithography
SVF	Stromal vascular fraction
TE	Tissue engineering
TIVA	Total Intravenous Anesthesia
UCS	Ultimate compressive strength
UV	Ultraviolet
VEGF	Vascular endothelial growth factor
YM	Young's Modulus

LIST OF FIGURES

LIST OF TABLES

1. INTRODUCTION

Three-dimensional (3D) printing, which is regarded as an efficient tool in tissue engineering (TE), has initiated a significant revolution in the fields of medicine and life sciences. Moreover, by using computer-aided manufacturing (CAM) and computer-aided design (CAD) tools, 3D bioprinting technology precisely places cells and biomaterials in predefined localities to form TE scaffolds. By using various additive manufacturing techniques such as inkjet printing, laser-based printing, bioextrusion, and photopolymerization, the developments in tissue engineering have allowed the manufacturing of more multifaceted 3D scaffolds, which include extracellular matrices, several cell types, and biomolecules as well (Li et al., 2017a). Noting that the ideal scaffolds in tissue engineering should match precisely the shape of the damaged area, and should have indispensable properties such as biodegradability, porosity, and biocompatibility. Therefore, the scaffolds used for regenerative treatments can repair lesions of various thicknesses and sizes by integrating with the existing native tissues (Li et al., 2017).

To achieve the production of functional tissue, which is the goal of tissue engineering, tissue scaffolds are subjected to in vivo experiments following in vitro experiments. However, for this, the biomaterials to be used must be sterilized and fabricated according to the in vivo damage model, and then chemical or photochemical cross-linking must be ensured and then implanted in the in vivo animal model under sterile conditions. Considering the changes that may occur in the damaged model, in addition to the loss of time and high cost, it is believed that direct bioprinting of the damaged tissue by *in situ* application using three-dimensional (3D) printing technology is considered a promising approach instead of the two-step in vitro experiments followed by the in vivo experiments. As for, *in situ* printing aims to bring tissue engineering one step closer to clinical applications (Agostinacchio et al., 2021; Akilbekova & Mektepbayeva, 2017).

The traditional clinical treatment of bone defects mainly depends on donor availability and usually includes several operations. Besides, using allogenic or autogenous bone grafts as therapeutic models is hindered by numerous obstacles including graft integration

and remodeling, limited volume availability, donor site morbidity, and the absence of osteogenic characteristics or structural capability. Hence, the 3D bioprinting technology stands as a great potential therapeutic tool for such injuries and clinical challenges, as it is able to repair tissue and organ structures. The current approach for 3D bioprinting to create a functional tissue in vitro before implantation is to culture cells in the scaffold fabricated by introducing materials using additive manufacturing technology and modulating agents (Badylak & Nerem, 2010; Briquez et al., 2015; Mertz, 2017) .

However, there are some problems with this method and with the clinical applicability of tissue conjugates produced by 3D printing/bioprinting in vitro, where they require several weeks to complete the whole process before scaffold implantation in vivo, which in turn hinders the clinical application of 3D bioprinting. Additionally, bioreactor systems are needed for the necessary biomimetic stimulations to ensure functionality after tissue suppression (Murdock & Badylak, 2017); (Villa et al., 2015).

Furthermore, 3D printing, culturing, and implantation processes of biomaterials that are frequently preferred in hydrogel structure and with low mechanical strength cause the morphology of the produced structure to deteriorate, and thus the failure of the one-to-one treatment planned according to the size and shape of the damage may occur (Villa et al., 2015). Considering all these disadvantages, a more effective therapeutic application for tissue regeneration can be achieved by providing the necessary biophysical and biochemical stimuli to the natural microenvironment of the tissue by performing *in situ* bioprinting directly on the damage.

2. LITERATURE SURVEY

2.1 Craniofacial Bone

Craniofacial bones play a crucial role in providing structural support and protection to vital organs such as the brain, eyes, and nasal cavity. These bones, including the frontal, parietal, occipital, temporal, maxillary, and mandible bones, form the intricate architecture of the skull and face. The craniofacial skeleton is essential for various physiological functions, including breathing, eating, and facial expressions. Defects or injuries in these bones can result from trauma, congenital anomalies, tumors, or surgical resections, posing significant challenges for reconstruction and rehabilitation (Emara & Shah, 2021); (Aghali, 2021); (Thrivikraman et al., 2017). Therefore, understanding the unique properties and regeneration potential of craniofacial bones is vital for advancing tissue engineering and regenerative medicine strategies aimed at addressing defects and injuries in this region.

2.1.1 Structure and function

Craniofacial bones are primarily composed of two types of bone tissue: compact (cortical) bone and spongy (trabecular) bone. The compact bone forms the dense outer layer, providing strength and rigidity, while the spongy bone consists of a porous, lattice-like structure that houses bone marrow and supports metabolic activities. These bones develop through two main ossification processes: intramembranous ossification, which forms the flat bones of the skull, and endochondral ossification, which forms the bones of the cranial base and facial skeleton (Zhang & Yelick, 2018).

The craniofacial skeleton's complex anatomy and functional requirements necessitate precise coordination of bone growth and remodeling. This dynamic process is regulated by various factors, including genetic signals, mechanical forces, and environmental influences.

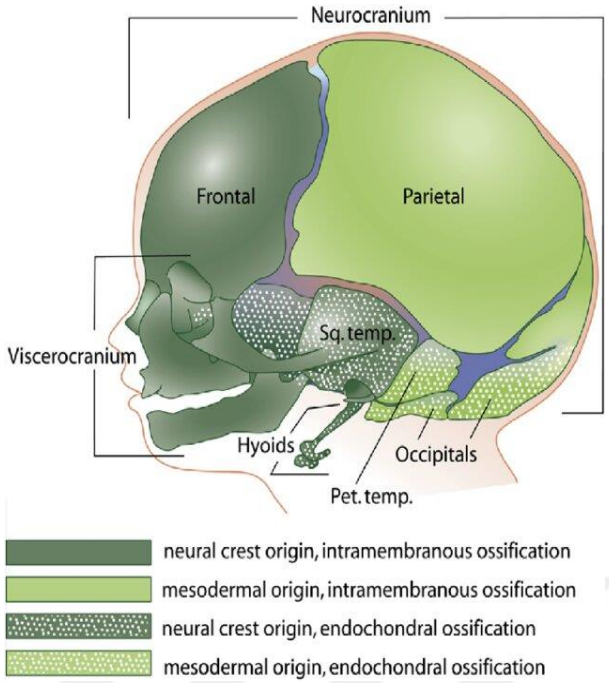

Figure 2.1 The craniofacial skeleton's complex anatomy and the formation of the craniofacial skeletal structures in the developing head. (Adapted from T.W. Sadler 2015) (Kruijt Spanjer et al., 2017)

The loss of craniofacial tissue can result from congenital conditions, such as clefting and craniofacial microsomia, or from acquired causes, such as facial trauma or tumor resection. This loss leads to significant aesthetic, functional, and psychological challenges. Additionally, disruptions in these processes can result in craniofacial deformities and functional impairments, which require advanced therapeutic interventions for effective reconstruction and regeneration (Chen et al., 2017).

In addition to their structural roles, craniofacial bones, like other bones in the body, contain bone marrow, which is essential for hematopoiesis. The unique anatomical features and the complex vascular network of these bones make them particularly challenging for regenerative strategies, highlighting the need for innovative approaches like *in situ* 3D bioprinting.

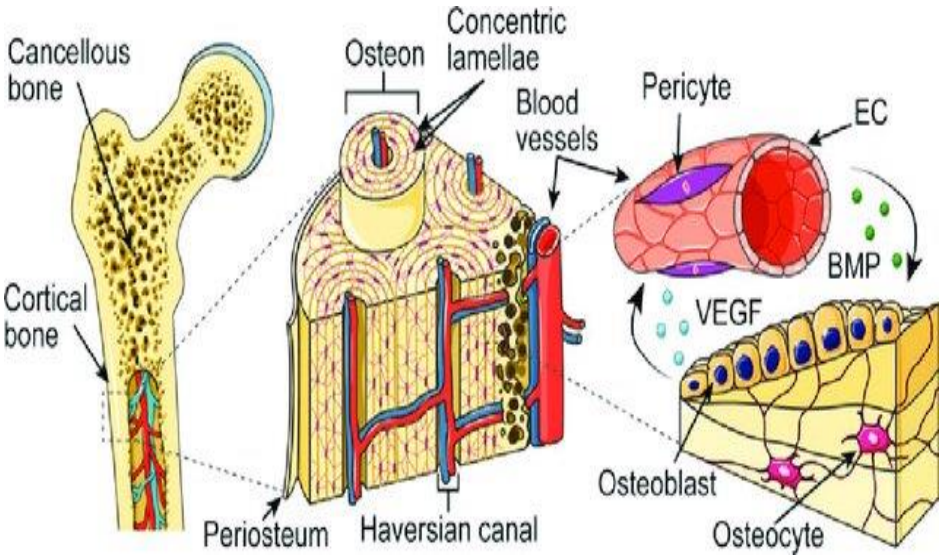

Figure 2.2 Schematic representation of bone structure showing how blood vessels are integrated into bone tissue to support the resident cells in both cancellous and cortical bone (Schott et al., 2021)

2.1.2 Clinical approaches for the regeneration of craniofacial bone

Natural bone tissue possesses the ability to remodel itself throughout life, although this capacity declines with age. This remodeling process is facilitated by the activity of osteoclasts and osteoblasts working antagonistically. Osteoclasts resorb bone tissue, and osteoblasts subsequently produce new bone tissue. This ongoing remodeling process regulates calcium homeostasis, repairs micro-scale fractures, and renews the skeletal structure.

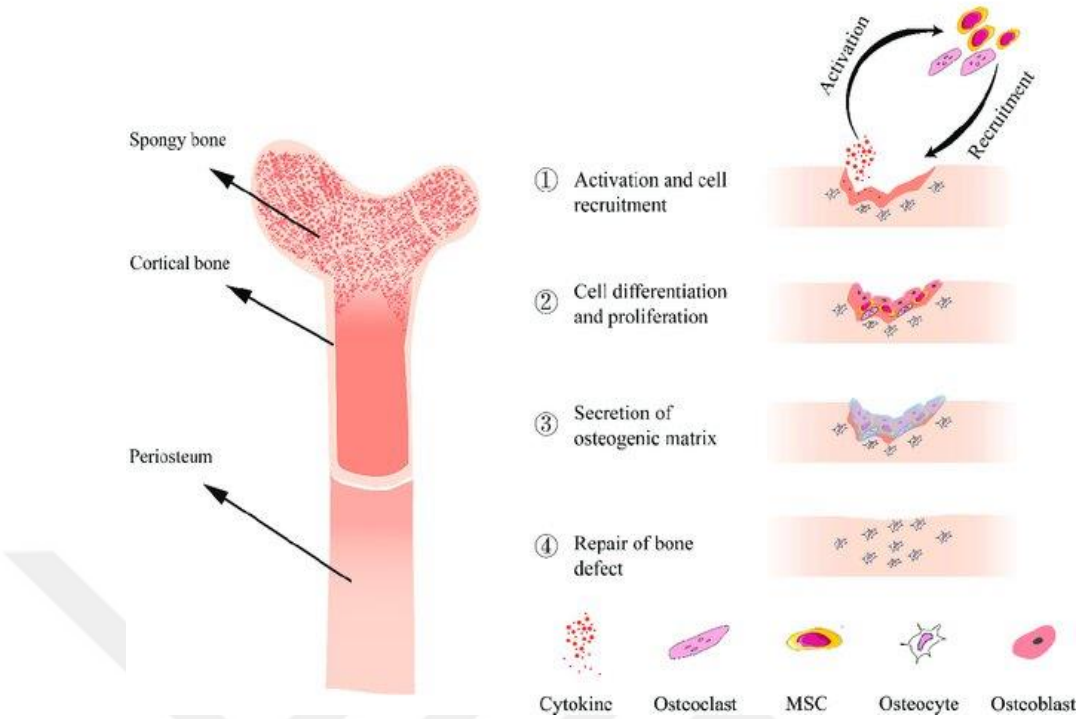

Figure 2.3 Schematic representation of the structure of bone (left) and bone repair process (right) (Feng et al., 2022)

Bone tissue can self-reconstruct and heal to some extent, a phenomenon known as "critical size defect." If a fracture is smaller than this critical size, bone tissue can regenerate without external intervention. The fracture healing process occurs in three major steps: inflammation, reparation, and remodeling. Immediately after a fracture, inflammation occurs, and a fibrin clot forms at the fracture site. Locally produced cytokines and growth factors within the hematoma facilitate the migration of osteoprogenitor cells to the defect site, guiding their differentiation into specific lineages such as chondroblasts and osteoblasts, which are responsible for forming hyaline cartilage and woven bone, respectively(Allori et al., 2008).These factors also regulate cell proliferation and the production of the extracellular matrix (ECM).

Clinical approaches to craniofacial bone regeneration have evolved significantly, driven by the need to address the limitations of traditional treatments such as autografts, allografts, and synthetic implants. Autografts, the gold standard for bone reconstruction, involve harvesting bone from the patient's own body, typically from the iliac crest. While autografts offer excellent biocompatibility and osteogenic potential, they are limited by

donor site morbidity, limited availability, and potential for significant pain and complications (Kim et al., 2008).

Allografts, which are derived from donor bone, provide an alternative but carry risks such as immunogenicity, disease transmission, and variable integration rates. On the other hand, synthetic implants, including metal and polymer-based materials, offer structural support but lack the biological cues necessary for effective bone regeneration and integration with the host tissue (Sutherland & Bostrom, 2005).Therefore, there is a growing interest in developing bioengineered solutions that combine biocompatibility, osteoconductivity, and osteoinductivity to enhance craniofacial bone regeneration (Younger & Chapman, 1989).

Moreover, it has been recognized that bone can regenerate and self-restore its functions without leaving any scar tissue, yet this is not always satisfactory. Various researchers reported that in most large bone defects, specifically those involving bone tumor resections or comminuted fractures, the regeneration potential of human bone is insufficient.

In today's clinical practice, various materials are utilized as grafts to fill these bone gaps. These grafts, which can be biological or synthetic, must meet essential requirements such as mimicking the porous structure of bone tissue and carrying osteoconductive factors and osteogenic cells. Biological materials like demineralized bone matrix and synthetic options such as hydroxyapatite and tricalcium phosphate are commonly used due to their ability to support bone growth and integration (Peterson et al., 2004).

Recent advances in tissue engineering and regenerative medicine have introduced the potential of using bioactive scaffolds, growth factors, and stem cells to enhance craniofacial bone repair. These approaches aim to create a conducive environment for new bone formation, promoting healing and functional restoration.

2.2 Tissue Engineering

Tissue engineering has emerged as a promising approach to address the limitations and complications associated with traditional methods of organ and tissue transplantation. Conventional techniques, including autografts, allografts, and xenografts, face significant challenges such as immune system reactions, disease transmissions, and the limited availability of suitable tissues for transplantation. Consequently, tissue engineering aims to replace damaged or failed organs and tissues with functional, healthy counterparts that are ready for transplantation (Khademhosseini & Langer, 2016).This interdisciplinary field combines principles from biological sciences and engineering to develop tissues that restore, maintain, or enhance tissue function (Mikos et al., 1993).

The process of tissue engineering involves several key steps. Initially, stem cells are harvested from the patient through surgical operations or biopsies and then multiplied in vitro. These cells are combined with scaffolds using various techniques. Once the integration of cells and scaffolds is achieved, often with the aid of the "artificially made tissue", it becomes ready for implantation into the patient’s damaged area.

The cells within the scaffold produce extracellular matrix (ECM), and the scaffold gradually degrades. This process ideally results in a bone repair environment that mimics the natural properties of bone tissue, which is porous and three-dimensional. Such architectures support osteoprogenitor cell proliferation, vascularization of the graft, and integration with the surrounding host bone, facilitating the remodelling process (Freyman et al., 2001).

In summary, tissue engineering aims to overcome the limitations of traditional transplantation methods by developing functional tissues and organs for transplantation. By integrating cells, scaffolds, and growth factors, tissue engineering provides a comprehensive approach to regenerating damaged tissues and restoring their functionality. This field holds significant promise for revolutionizing healthcare and offering innovative treatments for patients with tissue and organ deficiencies. Given the

constraints of existing treatment options, tissue engineering strategies have attracted significant research attention (Yang et al., 2017).

In addition, multidisciplinary research teams with expertise in biology, engineering, medicine, and regulatory affairs are essential for successfully navigating the complex path from the laboratory to the clinic. By overcoming these obstacles, tissue engineering can realize its maximum potential to revolutionize healthcare and provide innovative treatments for patients with tissue and organ deficiencies (Shafiee & Atala, 2017).

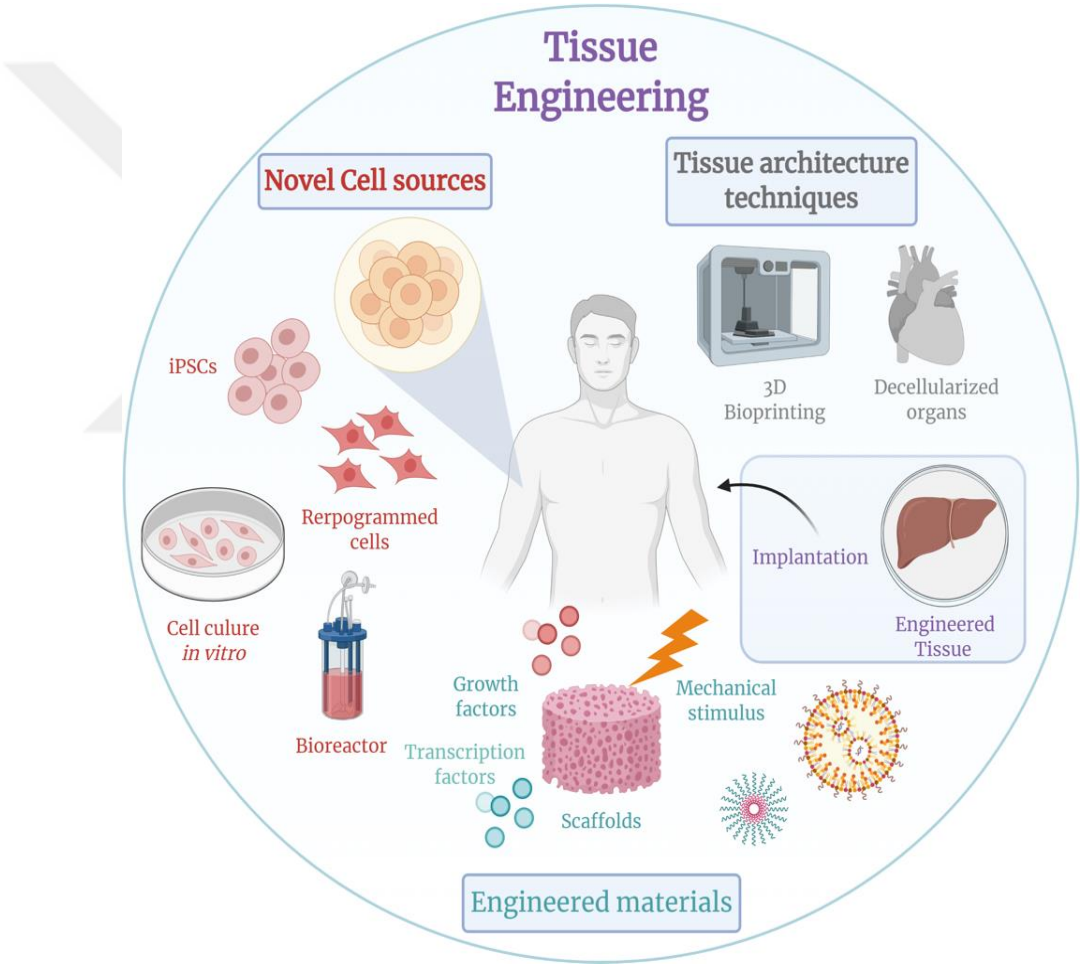

Figure 2.4 Schematic representation of tissue engineering (Designed by Biorender)

2.2.1 Overview of tissue engineering for bone

Bone tissue engineering is an advanced field and a subfield of tissue engineering that focuses on developing complex bone tissue constructs, including cortical, cancellous, or a combination of both types of bone tissues in order to restore damaged bone structures. Bone tissue engineering begins with the isolation of stem cells, where the choice of cells for this purpose depends on the target tissue and can include autologous cells from the patient or allogeneic cells from donors. Stem cells are particularly valuable in bone tissue engineering due to their ability to differentiate into various cell types, which is crucial for reconstructing different bone tissues (Gazit et al., 2019). These cells are harvested through surgical procedures or biopsies and then expanded in vitro, and then seeded onto a biodegradable scaffold (often created using advanced 3D printing techniques) that meets the mechanical requirements of the defect site. It is crucial that the scaffolds used in tissue engineering applications are biocompatible with the human body (Furth & Atala, 2014).

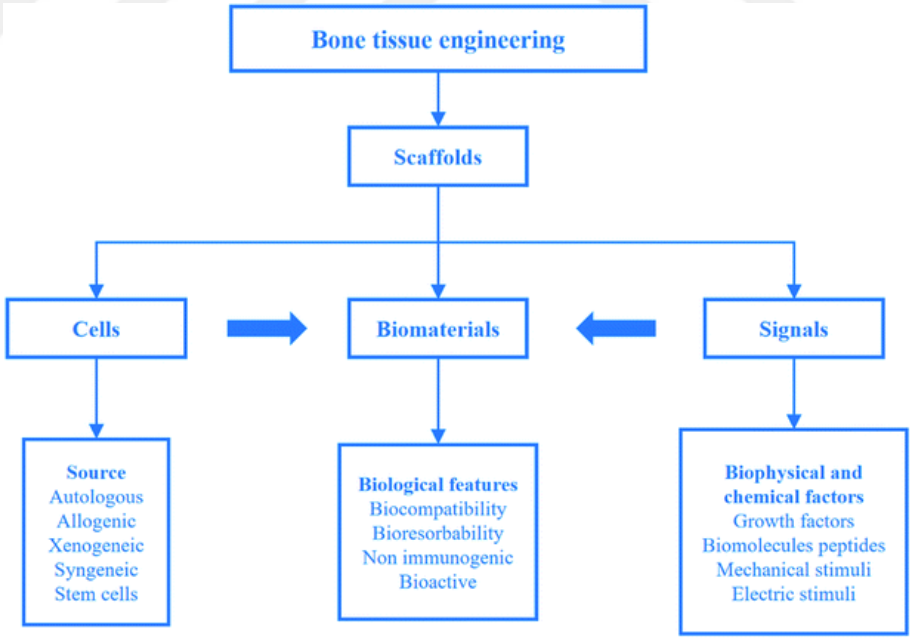

Figure 2.5 Strategies for bone tissue engineering (Qu et al., 2019)

Scaffolds are essential for providing structural support and ensuring the viability and functionality of the cells. They can be made from natural polymers such as collagen or synthetic materials like poly(lactic-co-glycolic acid) (PLGA), Alginate (Alg) and polycaprolactone (PCL). While natural polymers offer good biocompatibility, they may lack sufficient mechanical strength. Synthetic polymers, although stronger, may have lower biocompatibility. To address these challenges, researchers are exploring composite materials that combine the benefits of both types (Dhandayuthapani et al., 2011).

Hydrogels, which are water-swelling, cross-linked polymeric networks, have shown promise in bone tissue engineering. They can be derived from natural or synthetic polymers and offer flexibility in terms of shape and application. Hydrogels can be used to deliver growth factors or other bioactive molecules, enhancing their effectiveness in bone regeneration. However, ensuring their mechanical stability and long-term functionality remains a challenge (Luo et al., 2023).

2.2.2 Scaffolds for bone tissue engineering

Scaffolds are fundamental components in bone tissue engineering, serving as the structural foundation for new bone formation. The choice of biomaterials for scaffold construction is crucial, as these materials must be biocompatible, biodegradable, and possess appropriate mechanical properties while maintaining a porous, three-dimensional structure. Both natural and synthetic polymers are commonly employed in scaffold design, each offering unique advantages and limitations (Qu et al., 2019).

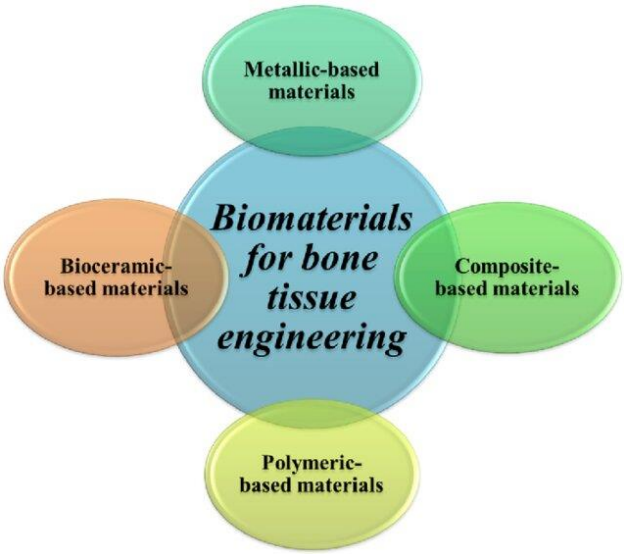

Figure 2.6 Biomaterials-based scaffolds for bone tissue engineering (Abu Owida et al., 2023)

Natural polymers, derived from biological sources such as plants, animals, or fungi, are favored for their high biocompatibility and low toxicity. They closely mimic the natural extracellular matrix, promoting cell attachment and growth. However, their structural complexity and the lengthy, costly extraction processes can be limitations (Muhamad & Lazim et al., 2014).Examples of natural polymers used in bone tissue engineering include collagen, gelatin, alginate, and chitosan. Collagen and gelatin, being key components of the extracellular matrix, are particularly effective in supporting cellular interactions and promoting tissue regeneration. Alginate and chitosan also offer good biocompatibility and stability, making them suitable for various applications (Malafaya et al., 2007).

Synthetic polymers, on the other hand, provide advantages such as ease of fabrication, cost-effectiveness, and the ability to tailor mechanical properties to specific requirements. These polymers are well-suited for 3D printing applications due to their thermoplastic behavior, although they may present challenges such as stiffness mismatch with native bone tissue and limited suitability as bioinks (Kellomäki et al., 2000).

Recent trends in scaffold development include the use of hybrid materials, which combine natural and synthetic polymers to leverage the benefits of both types while mitigating their respective drawbacks. This approach aims to create scaffolds with enhanced

properties that better meet the requirements of bone tissue engineering (Panwar & Tan, 2016) **Table 2.1** summarizes commonly used natural and synthetic polymers in scaffold fabrication for bone tissue engineering.

Table 2.1 Common Biomaterials for Bone Tissue Engineering

Natural Polymers	**Synthetic Polymers**
Collagen	Poly(lactic acid) (PLA)
Gelatin	Polycaprolactone (PCL)
Alginate	Poly(glycolic acid) (PGA)
Chitosan	Polyethylene glycol (PEG)

2.2.2.1 Alginate

Alginate is a naturally occurring polysaccharide derived from brown seaweed and is widely used in tissue engineering due to its favorable properties as a bioink. It is composed of β-D-mannuronic acid (M) and α-L-glucuronic acid (G)(Jovic et al., 2019; Malikmammadov et al., 2018) and is renowned for its biocompatibility, making it a prime candidate for various tissue engineering applications, including craniofacial bone regeneration (Lee et al., 2020).

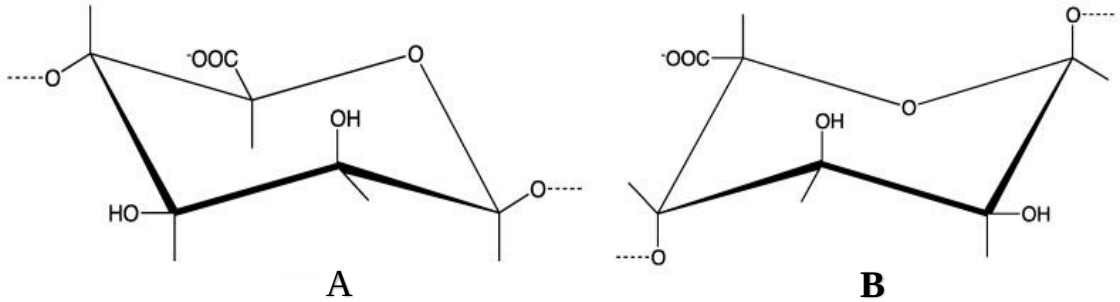

Figure 2.7 The structural components of alginate block varieties (A) β-(1–4)-d-Mannuronic acid; (B) α-(1–4)-l-Guluronic acid (Axpe & Oyen, 2016a)

Alginate gels are formed through ionic cross-linking, typically with calcium ions, leading to the formation of a stable, three-dimensional network that can support cell attachment and proliferation. The unique properties of alginate hydrogels include their biodegradability and tunable mechanical properties. Alginate can be easily modified to alter its gelation rate and mechanical strength, making it versatile for various tissue engineering applications (Farshidfar et al., 2023). Additionally, its ability to encapsulate cells and bioactive molecules enhances its suitability for regenerative medicine.

In bone regeneration applications, alginate is particularly advantageous due to its ability to form hydrogels through ionic cross-linking with divalent cations such as calcium ions (Ca^{2+}). This cross-linking process occurs under mild conditions compatible with physiological environments, maintaining cell viability within printed scaffolds. This adaptability allows for the fabrication of various structures, including hydrogels and scaffolds of different sizes and shapes, which can be tailored for specific bone repair needs (Lee et al., 2020).

Despite its benefits, alginate-based hydrogels can exhibit limitations in mechanical strength and stiffness, which are critical for bone regeneration. For instance, while alginate maintains chondrocyte morphology and phenotype effectively, its rapid gelling properties with calcium ions can result in reduced scaffold stiffness and size shrinkage, which may be suboptimal for supporting the mechanical demands of bone tissue (Axpe & Oyen, 2016b).

To address these limitations, researchers often combine alginate with other polymers to enhance its mechanical properties and functionality. Examples include collagen, methylcellulose, agarose, hydroxyapatite (HAp), chitosan, gelatine, and fibrinogen. These combinations aim to improve the structural integrity and durability of alginate-based materials, making them more suitable for applications requiring higher mechanical strength and biocompatibility (Wu et al., 2018).

2.2.2.2 Hydroxyapatite

Hydroxyapatite (HAp) is a naturally occurring mineral form of calcium apatite, with the formula $Ca_{10}(PO_4)_6(OH)_2$. It is the principal mineral component of bones and teeth, making it highly relevant for bone tissue engineering and regenerative medicine. HAp is well-known for its excellent biocompatibility, bioactivity, and osteoconductivity. (Liu et al., 2003). Structurally, HAp mimics the mineral phase of natural bone, which contributes to its ability to support bone ingrowth and integration. Its crystal lattice structure allows it to bond directly with bone tissue, enhancing the mechanical stability and biological performance of composite biomaterials used in bone repair and regeneration (Su et al., 2024).

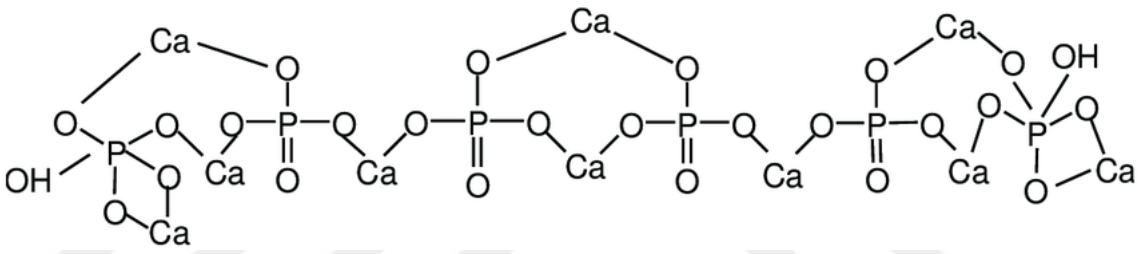

Figure 2.8 The structural components of hydroxyapatite (HAp), showing the arrangement of calcium (Ca^{2+}), phosphate (PO_4^{3-}), and hydroxide (OH^-) ions

In the context of craniofacial bone regeneration, the integration of alginate with hydroxyapatite (HAp) has proven particularly beneficial. Hydroxyapatite enhances the mechanical strength and osteoconductivity of the alginate scaffold, promoting better bone formation and repair. This combination leverages the advantages of alginate's printability and biocompatibility while addressing its limitations through the inclusion of HAp, thus providing a robust solution for effective craniofacial bone regeneration (Suo et al., 2021).

Table 2.2 Enhancements provided by hydroxyapatite (HAp) integration in alginate-based bioinks

Aspect	Enhancement from HAp Integration
Mechanical Properties	Improves mechanical strength and stiffness, making hydrogels suitable for load-bearing applications and mimicking natural bone tissue.
Bioactivity	Enhances osteoblast differentiation and bone formation, providing osteoconductive properties that support better integration with host bone.
Mineralization	Stimulates calcium and phosphate deposition, promoting mineralization and formation of new bone tissue.
Bioink Compatibility	Improves rheological properties, making the bioink more suitable for precise 3D bioprinting and creating complex bone structures.

Overall, the integration of hydroxyapatite with alginate hydrogels combines the best features of both materials, resulting in an enhanced bioink that supports effective bone regeneration and provides a more robust scaffold for tissue engineering applications (Iglesias-Mejuto & García-González, 2021)

2.3 3D Printing Techniques for Bone Regeneration

2.3.1 3D Printing

3D printing, also known as additive manufacturing (AM) or rapid prototyping, has revolutionized bone tissue engineering by enabling the precise creation of scaffolds

tailored to patient-specific needs. This technology transforms digital 3D models into physical objects through a layer-by-layer material deposition process, allowing for high customization and complexity in scaffold design

The 3D printing process in medical applications typically begins with the acquisition of patient-specific anatomical data through imaging techniques such as X-ray, computed tomography (CT), or magnetic resonance imaging (MRI) (Aimar et al., 2019). The acquired images undergo a segmentation process to isolate the targeted area, which is then used to create a 3D digital model. This model is designed using computer-aided design (CAD) software, which is essential for creating precise and accurate structures. Once the design is finalized, it is converted into an STL file format, which is compatible with 3D printers (Dawood et al., 2015).

3D printing allows for the creation of scaffolds that match the exact dimensions and anatomical features of the defect site, ensuring a better fit and integration with the surrounding tissue. This customization is achieved by using imaging data to generate precise digital models, which are then printed to produce the scaffold (Derby, 2012). Additionally, this technology supports a wide range of biomaterials, including metals, ceramics, and polymers. Each material offers unique advantages for bone regeneration. For example, bioceramics like hydroxyapatite promote osteoconductivity, while polymers such as poly (lactic-co-glycolic acid) (PLGA) provide degradability that aligns with the natural bone healing process (Hasirci V., 2007).

3D printing excels at creating complex structures with controlled porosity, which is crucial for tissue engineering. Porous scaffolds facilitate cell migration, nutrient and oxygen diffusion, and waste removal, closely mimicking the natural extracellular matrix of bone. The iterative nature of 3D printing allows for rapid prototyping and production, significantly reducing the time from design to fabrication. This rapid turnaround is beneficial in clinical settings where timely intervention is critical. Furthermore, 3D printing enables the incorporation of bioactive molecules such as growth factors, drugs, and stem cells into the scaffolds. These molecules can be precisely positioned within the scaffold to promote targeted tissue regeneration and healing (Compaan et al., 2017).

Various 3D printing methods have been developed, each with its own advantages and applications, including stereolithography (SLA), fused deposition modeling (FDM), selective laser sintering (SLS), and selective laser melting (SLM) (H. J. Chen, 2012). Each method varies in terms of material compatibility, resolution, and production speed, making it essential to choose the appropriate technique based on the specific requirements of the medical application (Moreno Madrid et al., 2019).

In summary, 3D printing is a transformative technology in bone tissue engineering, offering unparalleled precision, customization, material versatility, and the ability to create complex, porous structures. These attributes make it an invaluable tool for developing effective scaffolds for bone regeneration.

2.3.2 Bioprinting

Bioprinting is an emerging and multidisciplinary technology that evolved from 3D printing. The origins of 3D printing can be traced back to 1984 when Charles W. Hull developed stereolithography (SLA) for creating three-dimensional objects. In 1988, Robert J. Klebe demonstrated the potential of positioning biological products using a Hewlett Packard inkjet printer and a graphic plotter, laying the groundwork for bioprinting (Klebe, 1988; Ozbolat et al., 2017; Saygili et al., 2020). Later, in 1999, David J. Odde and Michael J. Renn printed living cells using 3D laser bioprinting, showcasing the feasibility of synthesizing tissues with complex anatomies (Odde & Renn, 1999; Ozbolat & Hospodiuk, 2016). The early 2000s saw further advancements, such as Rolf Muelhaupt's work on three-dimensional plotting of thermosensitive gels and the development of the first extrusion-based bioprinter by Landers et al. in 2002, marketed as the "3D-Bioplotter." Subsequent innovations included adapting inkjet printers for cell printing by Boland et al. in 2003, and the addition of an electro-hydrodynamic jet by Suwan N. Jayasinghe in 2006 to deposit living cells (Gu et al., 2020; Landers et al., 2002; Landers & Mülhaupt, 2000; Wilson & Boland, 2003) Significant milestones also include the synthesis of vascular tissue by Narotte et al. in 2009, *in situ* bioprinting by Skardal and colleagues in 2012, and recent advancements such as adding chondrogenic progenitor cells to hydrogels for cartilage regeneration and developing methods for pre-vascularized

tissue manipulation (Norotte et al., 2009; Skardal et al., 2012). Finally, Ramasamy et al. (2021) created an artificial skin using an extrusion-based 3D bioprinter. The goal of this research was to explore the possibility of producing full thickness reconstructed human skin in a consistent and scalable way (Nulty et al., 2021; Ramasamy et al., 2021; Zhou et al., 2021).

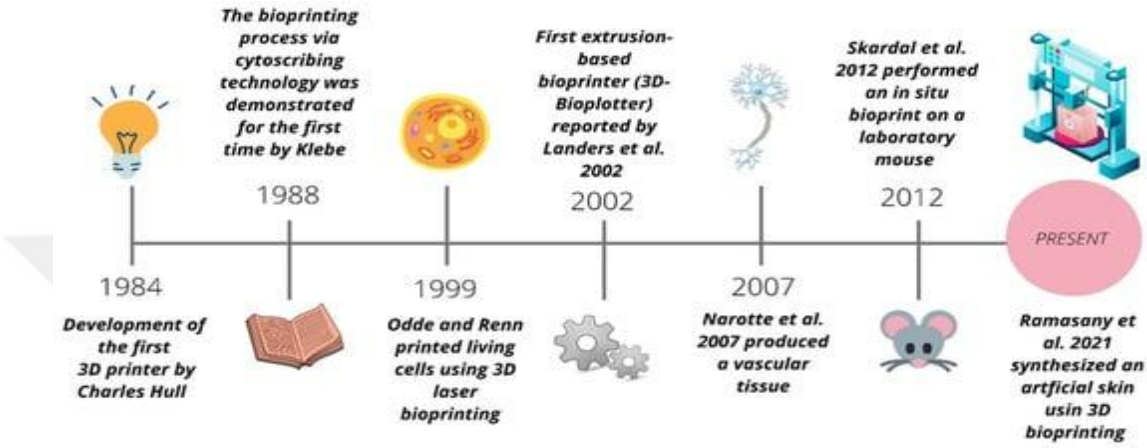

Figure 2.9 Evolution of 3D bioprinting process (Landers et al., 2002; Norotte et al., 2009; Ramasamy et al., 2021; Skardal et al., 2012; Lima et al., 2022)

Bioprinting, which is considered a subset of 3D printing, involves the precise placement of cells, biomaterials, and bioactive molecules in a layer-by-layer manner to create tissue constructs that mimic the architecture and function of natural tissues. This advanced technique holds significant promise for bone regeneration, allowing for the creation of complex structures that closely replicate the native bone environment. The process begins with the creation of a digital model of the tissue or organ to be printed, derived from medical imaging data like CT or MRI scans, which provide detailed information about the patient's anatomy. This digital model guides the bioprinter in the precise deposition of bioinks—mixtures of living cells and supportive biomaterials—onto a substrate (Zhang et al., 2021).

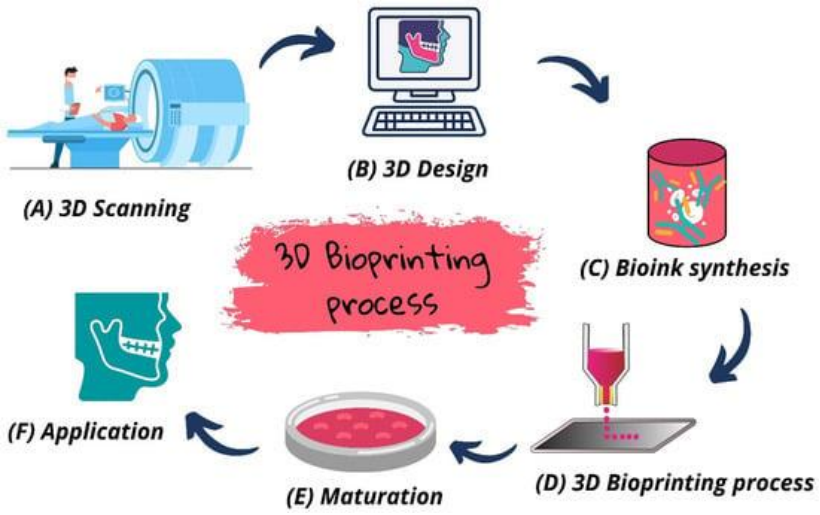

Figure 2.10 Stages of the 3D bioprinting process (Lima et al., 2022)

Bioinks are crucial in bioprinting as they provide the necessary environment for cell viability, proliferation, and differentiation. Commonly used biomaterials in bioinks include natural polymers like alginate, collagen, and gelatin, as well as synthetic polymers such as poly (ethylene glycol) (PEG) and polycaprolactone (PCL). Natural polymers are favored for their biocompatibility and ability to support cell functions, while synthetic polymers offer greater control over mechanical properties and degradation rates (Heid & Boccaccini, 2020; Jakus et al., 2016).

Bioprinting offers several advantages for bone tissue engineering. One primary benefit is the ability to create scaffolds with high precision and complexity, allowing for the incorporation of vascular networks essential for nutrient and oxygen delivery within the tissue construct. This vascularization is critical for the survival and function of the printed bone tissue, particularly in larger constructs. Furthermore, bioprinting enables the spatial patterning of multiple cell types within a single construct, which is essential for recreating the hierarchical structure of bone. This includes the ability to print osteoblasts (bone-forming cells), osteoclasts (bone-resorbing cells), and endothelial cells (which form blood vessels) in specific arrangements that promote proper bone formation and remodeling (Sutherland & Bostrom, 2005).

The use of growth factors and other bioactive molecules in bioinks can further enhance the regenerative capabilities of bioprinted constructs. These molecules can be precisely positioned within the scaffold to promote cell differentiation, tissue maturation, and integration with the host tissue (Spencer et al., 1991).

Bioprinting technologies include inkjet bioprinting, microextrusion bioprinting, and laser-assisted bioprinting, each offering unique advantages in terms of resolution, speed, and cell viability. Inkjet bioprinting is noted for its high speed and suitability for large-scale production, whereas microextrusion bioprinting provides excellent control over the deposition of highly viscous bioinks. Laser-assisted bioprinting offers high resolution and cell viability but is typically limited to smaller constructs (Ventura, 2021).

In conclusion, bioprinting represents a cutting-edge approach in bone tissue engineering, providing the ability to create highly precise, complex, and functional bone constructs. This technology leverages advanced biomaterials and cellular engineering to develop innovative solutions for bone regeneration, with significant potential for clinical translation (Lima et al., 2022).

2.3.3 Bioinks

Bioinks are fundamental to the bioprinting process, serving as the medium that carries and supports living cells during and after printing. The development and optimization of bioinks are critical for the success of bioprinted constructs, especially in the context of bone tissue engineering. Bioinks must meet several criteria: biocompatibility, printability, mechanical integrity, and the ability to support cell proliferation and differentiation (Dzobo et al., 2019).

Biocompatibility is a primary requirement for bioinks, ensuring that the materials do not elicit adverse immune responses and are conducive to cellular functions. Common biocompatible materials used in bioinks include natural polymers such as alginate, collagen, gelatin, and hyaluronic acid. These materials closely mimic the natural

extracellular matrix (ECM) and provide an environment that supports cell attachment, proliferation, and differentiation (Abdollahiyan et al., 2020).

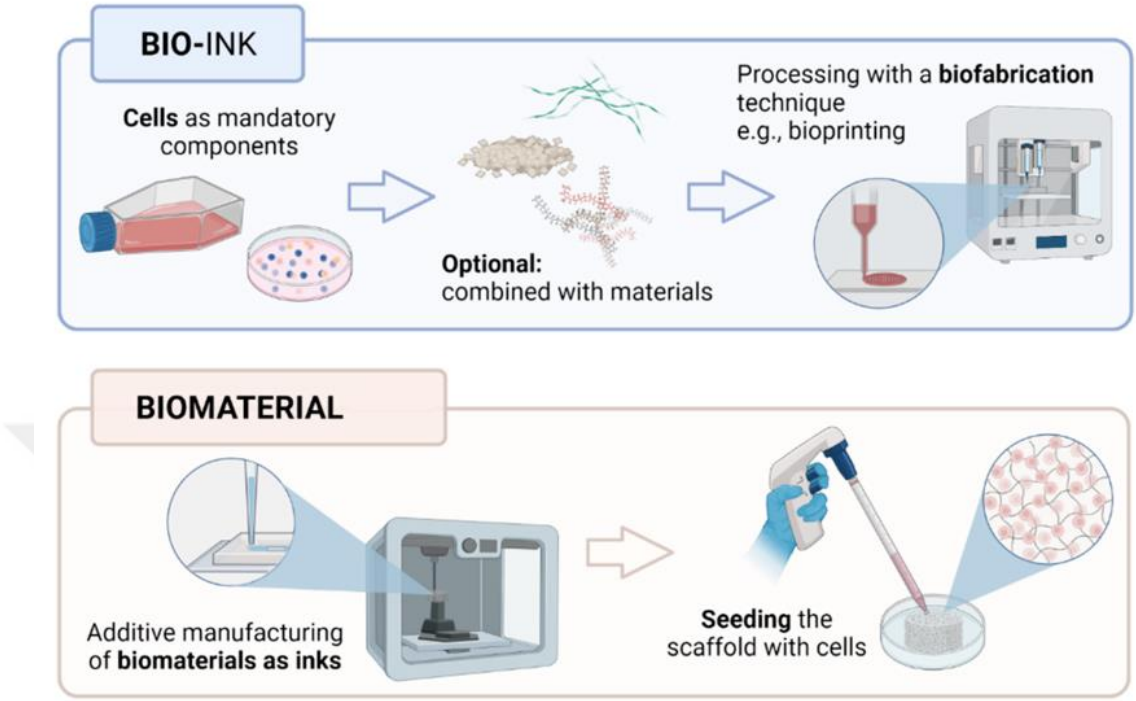

Figure 2.11 Distinction between a bio-ink (i.e., cell-laden) and a biomaterial (i.e., cell-free). (Lima et al., 2022)

Alginate, for instance, is widely used due to its biocompatibility, ease of gelation, and ability to form hydrogels under mild conditions. It supports cell viability and is often used in combination with other materials to enhance its mechanical properties and bioactivity. While collagen and gelatin, both derived from ECM proteins, provide excellent cell adhesion sites and promote cellular functions. Hyaluronic acid (HA), another natural polymer, is known for its role in tissue hydration and cellular signaling, making it a valuable component of bioinks for bone tissue engineering (Naghieh & Chen, 2021).

Synthetic polymers are also utilized in bioinks for their tunable mechanical properties and controlled degradation rates. These materials can be engineered to possess specific characteristics that enhance the structural integrity of the printed constructs and provide a controlled environment for cell growth and differentiation (Murphy & Atala, 2014)

However, synthetic polymers often require modification to improve their bioactivity and compatibility with cells.

Hydrogels, formed from both natural and synthetic polymers, are particularly important in bioink formulations due to their high-water content and ability to mimic the hydrated nature of native tissues. Hydrogels provide a supportive matrix that facilitates nutrient and oxygen diffusion to the encapsulated cells, promoting their survival and function (Cui et al., 2020).

The incorporation of bioactive molecules, such as growth factors, cytokines, and signaling peptides, into bioinks can further enhance their performance. These molecules guide cellular behaviors, including proliferation, migration, and differentiation, which are crucial for successful tissue regeneration. For bone tissue engineering, growth factors like bone morphogenetic proteins (BMPs) and vascular endothelial growth factor (VEGF) are often included to promote osteogenesis and angiogenesis (Reddi & Reddi, 2009).

The printability of bioinks, defined by their rheological properties and ability to maintain shape fidelity post-printing, is another critical consideration. Bioinks must possess suitable viscosity and shear-thinning behavior to be extruded smoothly through the printer nozzle and form stable structures upon deposition. Crosslinking methods, such as ionic, thermal, or photo-induced crosslinking, are employed to stabilize the printed constructs and maintain their architecture during the maturation process (Fatimi et al., 2022).

In summary, bioinks are integral to the success of bioprinting in bone tissue engineering, providing the necessary support and environment for cell viability and function. The selection and optimization of bioinks, combining natural and synthetic polymers with bioactive molecules, enable the creation of complex and functional bone constructs. Advances in bioink formulations continue to enhance the capabilities of bioprinting, paving the way for innovative solutions in regenerative medicine (Murphy & Atala, 2014).

2.4 In Situ 3D Bioprinting

In situ 3D bioprinting represents a transformative approach in tissue engineering, enabling the direct printing of cells and biomaterials onto defect sites within the body. This technique aims to address the limitations of traditional tissue engineering methods by facilitating precise cell placement, minimizing the need for extensive in vitro culture, and enhancing the integration of the engineered tissue with the native tissue. The process involves the use of bioprinters that can be operated in a surgical setting, allowing for real-time tissue construction during medical procedures (Li et al., 2017b).

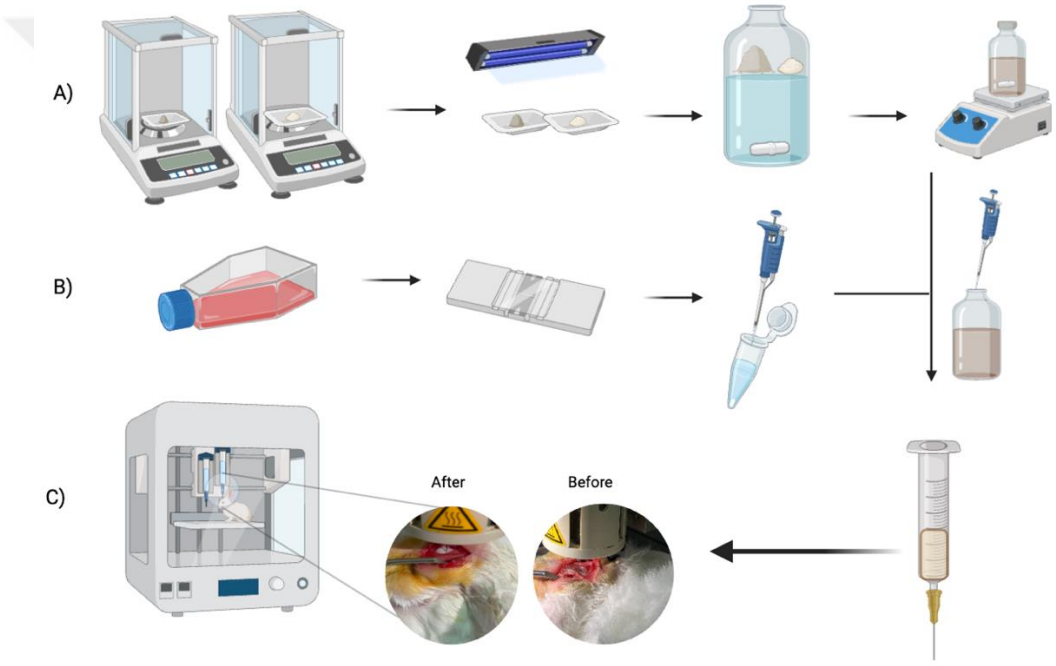

Figure 2.12 Illustration of *in situ* 3D bioprinting; A) Bioink Preparation, B) Cell Collection & Culturing, C) In situ bioprinting (Designed by Biorender)

The primary advantage of *in situ* 3D bioprinting is its ability to create customized tissue constructs that conform to the specific geometry of the defect site. This level of precision is particularly beneficial for craniofacial bone regeneration, where complex anatomical structures must be accurately replicated. The *in situ* approach also reduces the risk of contamination and cell damage that can occur during the transfer of prefabricated constructs from the laboratory to the patient.

In situ bioprinting typically involves several key components: a bioprinter equipped with multiple printheads, bioinks tailored for the target tissue, and imaging systems to guide the printing process. The bioprinter must be capable of precise control over the deposition of cells and materials, often using techniques such as inkjet, extrusion, or laser-assisted printing. Imaging technologies, such as real-time optical coherence tomography (OCT) or magnetic resonance imaging (MRI), provide the necessary feedback to ensure accurate alignment and integration of the printed tissue (Murphy & Atala, 2014).

Bioinks used in *in situ* bioprinting must meet stringent criteria to ensure biocompatibility, printability, and mechanical stability. Alginate and hydroxyapatite-based bioinks are commonly used for bone tissue engineering due to their favorable properties. Alginate provides a supportive matrix for cell encapsulation and promotes cell viability, while hydroxyapatite enhances the osteoconductivity and mechanical strength of the printed constructs. The combination of these materials results in bioinks that can support the regeneration of craniofacial bone with improved structural integrity and functionality.

Applications of *in situ* 3D bioprinting extend beyond craniofacial bone regeneration to include other areas of the body, such as cartilage repair, skin grafting, and cardiovascular tissue engineering. The versatility of this technique allows for the creation of a wide range of tissue types, tailored to the specific needs of each patient. Case studies have demonstrated the potential of *in situ* bioprinting to enhance wound healing, reduce recovery times, and improve clinical outcomes (Briquez et al., 2015).

The clinical translation of *in situ* 3D bioprinting is supported by ongoing advancements in bioprinter technology, bioink formulations, and imaging systems. Researchers are continually exploring new materials and methods to optimize the performance of *in situ* bioprinting and expand its applications. Preclinical studies using animal models have shown promising results, paving the way for future clinical trials and the eventual adoption of this technique in routine medical practice (Li et al., 2021a).

In conclusion, *in situ* 3D bioprinting represents a significant advancement in tissue engineering, offering a precise, customizable, and efficient method for regenerating

complex tissues directly within the patient. The integration of advanced bioprinter technology, bioinks, and imaging systems is essential for the successful application of this technique, with ongoing research driving further improvements and expanding its potential. This innovative approach holds great promise for enhancing patient outcomes and transforming the field of regenerative medicine (Badylak & Nerem, 2010; Ma et al., 2020; Mertz, 2017).

2.4.1 Case studies and experimental models

The emergence of *in situ* 3D bioprinting has revolutionized tissue engineering, offering a transformative approach to tissue regeneration directly at the defect site. This technique allows for the precise deposition of bioinks, incorporating cells and biomaterials, in a manner that mimics the native tissue environment. The feasibility of *in situ* bioprinting in various experimental animal models across different tissues has been extensively demonstrated, highlighting its potential for clinical use, injury repair, and specifically the restoration of bone defects (Di Bella et al., 2018; Li et al., 2017b; Lipskas et al., 2019).

For example, Li et al. (2021) investigated the feasibility of repairing large segmental bone defects in a swine model using *in situ* 3D bioprinting technology with a robotic manipulator. Bioink gelation was systematically optimized under physiological conditions to achieve desirable mechanical properties suitable for bone regeneration. A D-H kinematic model was employed to enhance printing accuracy to 0.5 mm. Results showed improved treatment effects in the 3D bioprinting group after three months, concluding that robotic *in situ* 3D bioprinting holds promise for direct clinical application.

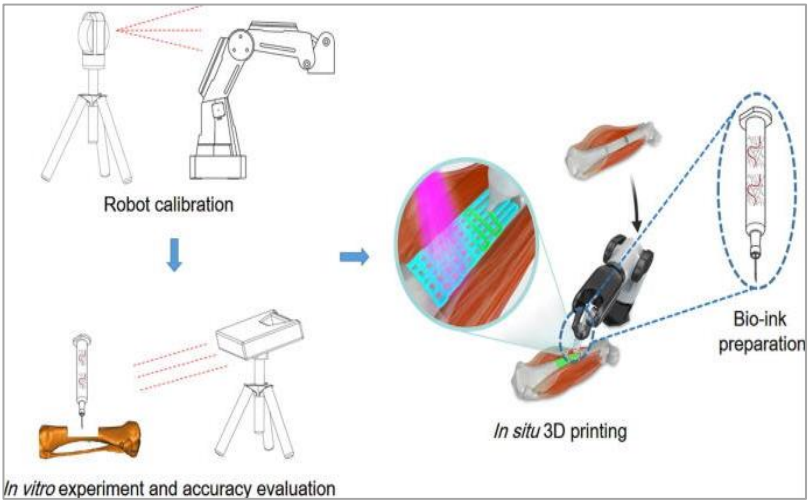

Figure 2.13 Whole process of *in situ* 3D bio-printing (Li et al., 2021)

In another study, Ma et al. (2020) applied modified hyaluronic acid (HAMA) for cartilage tissue regeneration in rabbits using a robotic-assisted *in situ* biosuppression system. The results indicated that cartilage injury could be effectively treated with this method, demonstrating the appropriateness of robotic-assisted *in situ* 3D bioprinting for improving surgical procedures and promoting cartilage regeneration (Ma et al., 2020).

For *in situ* bioprinting of bone damage, a computer and robotic-assisted laser 3D printer was developed, utilizing nano-hydroxyapatite (n-HA) for bone tissue healing. This new generation of 3D printers, created with advancing technology, enables the creation of cell-loaded bioactive scaffolds in a sterile environment, suitable for *in situ* printing.

Another application involved a 3D printer designed for *in situ* bioprinting to heal cartilage damage using GelMA and HAMA biomaterials, investigating its effect on osteochondral damage in sheep (Di Bella et al., 2018).

Li et al. (2017) also explored the combined application of 3D scanning and 3D printing for treating bone and cartilage defects. Three different defect models were created to mimic orthopedic diseases, followed by high-resolution 3D scanning to obtain 3D digital models of the defects and corresponding healthy parts. The study concluded that 3D

scanning and 3D bioprinting could provide a novel strategy for tissue engineering and regenerative medicine, as defects were restored perfectly *in situ* (Li et al., 2017b).

Preliminary data from these studies suggest that the *in situ* bioprinting approach is a promising regenerative strategy for clinical applications. This method enables the production of patient-specific 3D structured tissue constructs, offering rapid and effective regenerative therapy when combined with cells isolated during surgery.

2.5 Aim, Novelty and Approach of the Study

This study aims to develop a clinically translatable *in situ* 3D bioprinting strategy specifically for craniofacial bone regeneration. With significant advancements in 3D printing and bioprinting technologies, the research purposes to address and overcome the limitations associated with traditional bone regeneration methods. These traditional approaches often face issues such as limited availability of donor tissues, the need for multiple surgeries, and insufficient osteogenic properties. In contrast, the *in situ* 3D bioprinting method offers a transformative alternative by enabling the precise deposition of cells and biomaterials directly onto the damaged area, thereby creating customized tissue scaffolds that align perfectly with the shape and mechanical properties required for effective bone repair.

The core objective of this research is to develop a strategy that is not only effective in promoting bone regeneration but also practical for clinical use. This involves leveraging CAD and CAM tools to model and 3D print scaffolds directly onto the damaged tissues, eliminating the conventional two-step process of separate in vitro and in vivo experimentation. A significant novelty of this approach lies in its application of *in situ* bioprinting technology directly onto live animal models. This method provides a more accurate simulation of clinical conditions compared to ex vivo or isolated tissue models, thus enhancing the potential for successful clinical translation.

In this study, preclinical validation was conducted using a rabbit model, where critical-sized bone defects were induced on the parietal bones. An Alginate and Hydroxyapatite

bioink was then applied using a 3D bioprinter. Subsequent evaluations, including CT scans, histopathological analysis, and micro-CT imaging were performed to assess the effectiveness of the bone regeneration process. The results indicated successful bone healing and integration, demonstrating the efficacy of the *in situ* bioprinting technique.

By directly applying biophysical and biochemical stimuli to the damaged area, this approach provides a rapid, patient-specific, and effective regenerative therapy. The successful outcomes of this research contribute valuable evidence supporting the viability of *in situ* 3D bioprinting as a promising technique for craniofacial bone regeneration. Furthermore, this innovative method holds potential implications for broader clinical applications within the fields of tissue engineering and regenerative medicine, offering a new horizon for patient-specific therapeutic strategies.

3. MATERIALS AND METHODS

3.1 Materials

The materials used within the scope of this thesis and their intended use are presented in **Table 3.1.**

Table 3.1 The materials used, their suppliers and intended use within this thesis

Material	**Brand / Company**	**Intended Use**
ASC rabbit adipose cell line	Isolation Process	Cell-material interaction studies
Fibroblast growth factor (bFGF)	Sigma-Aldrich	ASC expansion medium
Fetal bovine serum (FBS)	Biological Industries	Cell culture medium
Penicillin streptomycin (P/S)	Biological Industries	Cell culture medium
Dulbecco's Modified Eagle Medium (DMEM) (high glucose)	Biological Industries	Cell culture medium
Trypsin	Biological Industries	Cell passaging
Dimethyl Sulfoxide (DMSO)	Sigma-Aldrich	Cell freezing

Table 3.1 The materials used, their suppliers and intended use within this thesis (continued)

Triton X100	Merck	Cell permeabilization
Tween20	Merck	Cell permeabilization
Bovine serum albumin (BSA)	Sigma-Aldrich	Model protein
Sodium alginate (medium viscosity)	Sigma-Aldrich	Scaffold production
Hydroxyapatite (HAp)	Sigma-Aldrich	Scaffold production
Calcium chloride ($CaCl_2$)	Sigma-Aldrich	Crosslinking
Ketamine (35 mg/kg)	Randlab	General Anesthesia
Xylazine (10 mg/kg)	Randlab	General Anesthesia
Ceftriaxone (50 mg/kg)	Randlab	Pre-operative Antibiotic
Meloxicam (1 mg/kg)	Randlab	Post-operative Antibiotic

3.2 Methods

The aim of this thesis is to develop a 3D *in situ* bioprinting strategy for the regeneration of bone defects with potential for future clinical translation. In this context, preclinical development and validation studies for *in situ* bioprinting applications were conducted to ensure the effectiveness and safety of the technique. These studies focused on optimizing bioink composition, refining printing parameters, and assessing biological outcomes using appropriate animal models. The main goal was to establish a robust foundation for the clinical application of *in situ* 3D bioprinting for bone regeneration.

3.2.1 Precision 3D scanning and digital modelling

By 3D scanning, the rabbit was scanned from three different angles to ensure that all surfaces of the craniofacial bone are captured by the camera. Preceding the scanning procedure, a minor haircut was administered to the rabbit to optimize the scanning process

for the targeted area. Subsequently, the scanned data was restored to STL format, and the shape of the 3D printing object was determined with reverse engineering software (e.g., Fusion 360 Software) in a few minutes.

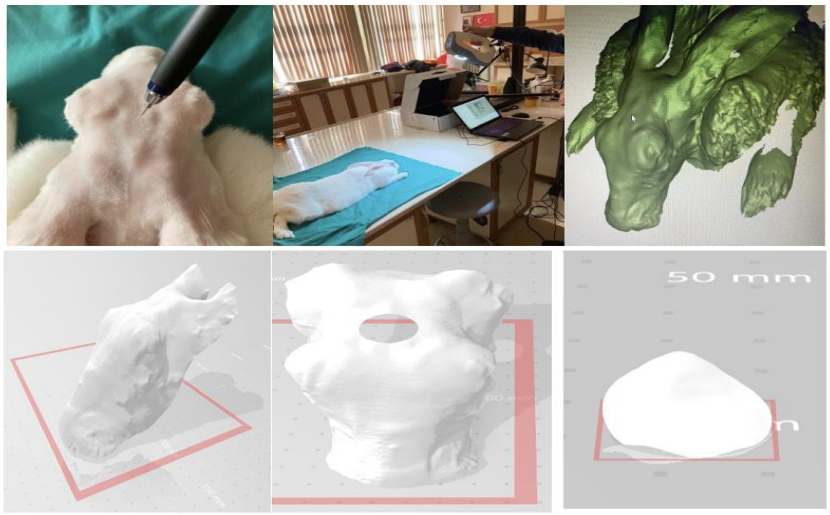

Figure 3.1 Workflow of Precision 3D Scanning and Digital Modelling for Craniofacial Bone

It is noteworthy that prior to and following the scanning process of the designated area, the exact position of the defect to be created was marked. Then, using Fusion 360, modifications were made to the scanned head model, where the defect was virtually created. Consequently, both the head model and the graft, intended to cover the defect area, were prepared for printing.

3.2.2 Optimization of in situ 3D printing strategies on rabbit models

The rabbit head model was fabricated through 3D printing utilizing the Ultimaker 2+ printer, using Polylactic Acid (PLA) filaments. Simultaneously, the bone grafts were printed through the melt extrusion technique, where PCL (Perstorp AB, Sweden) (Mw = 37000 g/mol) was melted in the high-temperature print head of the 3D Bioplotter® (EnvisionTec, Germany) at 130 °C. The molten PCL was extruded through a metallic 23G nozzle at 4.5 bar and 3D printed on a glass surface. Following fabrication, the graft

was strategically positioned over the head to check its ability to fully cover the designated defect area.

Figure 3.2 Fabrication of rabbit head model and PCL graft by 3D printing

Subsequently, to ensure the success of the *in situ* 3D printing process, several trials were conducted on smaller models to optimize the printing parameters, instead of doing it on complete head models and waste both time and material **(Figure 3.3)**. Finally, after precise preparation and optimization, *in situ* 3D printing was applied directly onto the complete head model using the determined optimal printing parameters **(Table 3.2**).

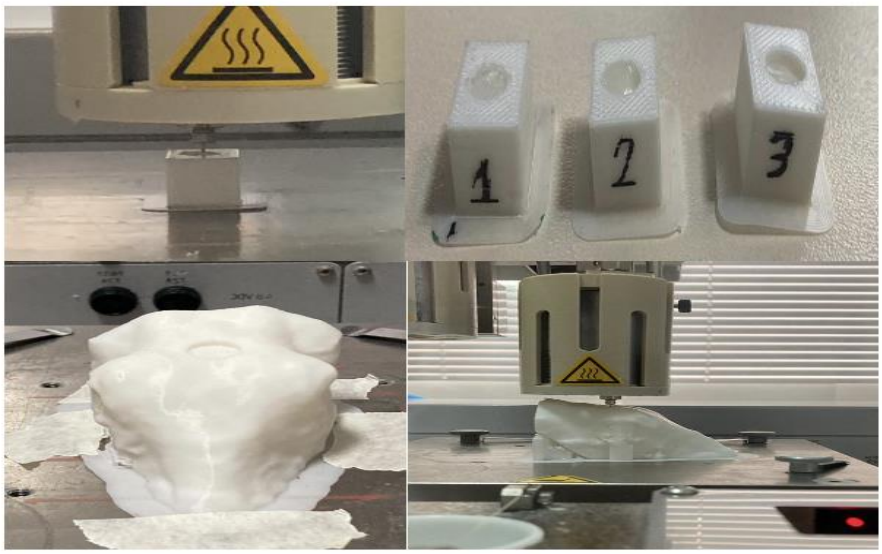

Figure 3.3 Application of optimized *in situ* 3D printing parameters on complete rabbit head model

The printing trials focused on determining the most effective conditions for printing on smaller models, allowing for precise preparation before application on the complete rabbit head model. The optimized parameters used for these trials are summarized in **Table 3.2**.

Table 3.2 Parameters for *in situ* 3D printing of PCL on rabbit head models (n=3)

Parameters						
Speed (mm/s)	3	3	3	2.5	2.5	2.5
Pressure (bar)	5.5	5.5	5.5	5.5	4.5	4.5
Temperature (°C)	130	130	130	130	130	130
Waiting Time (sec)	30	20	10	10	10	0

3.2.3 Optimization of the bioink

3.2.3.1 3D Printing optimization of alginate

Aqueous bioinks with three different alginate concentrations (6, 8 and 10 wt% with respect to water) were prepared using milliQ water as a solvent. All alginate solutions were prepared under vigorous agitation (500 rpm) using a magnetic stirrer (Ika®, Germany) for at least 1 h at room temperature (RT). The thus obtained alginate solutions were degassed in a sonication bath (Elma® Schmidbauer GmbH, Germany) for 10 min to eliminate air bubbles.

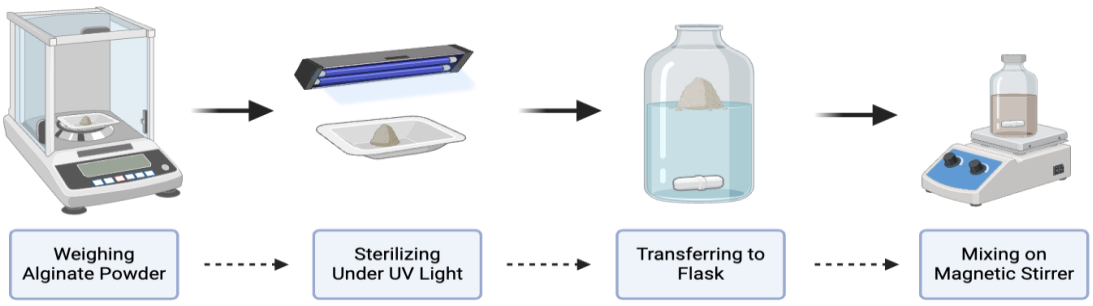

Figure 3.4 Preparation of sterile alginate solution (Designed with Biorender)

Hydrogels were obtained by printing the alginate inks with the 3D Bioplotter® (EnvisionTec, Germany) at RT using an extrusion printhead with a 3-mL syringe and a 330-µm nozzle (23 Ga Metallic Orange needle). Subsequently, *in situ* 3D printing was applied on the 3D head model, accompanied by a systematic optimization process for printing alginate. Multiple trials with various parameters (including the concentration of Alginate ranging between 6 – 10% & the pressure ranging between 1.5 – 3 bar) were performed. Finally, 3D printed alginate cylindrical scaffolds with dimensions of 8 x 8 x 5 mm were obtained. After the printing process, cross-linking of the bioink was achieved using a sterile 0.5 M $CaCl_2$ solution.

3.2.3.2 3D Printing optimization of alginate & hydroxyapatite

Different HAp concentrations (4, 8, 16 and 24 wt% with respect to water) were added to the 6 wt% alginate solutions. Then, the solutions were left overnight on the magnetic stirrer (Ika®, Germany) under vigorous agitation (500 rpm) at RT.

Scaffolds were obtained by printing the Alginate/Hydroxyapatite inks with the 3D Bioplotter® (EnvisionTec, Germany) at RT using an extrusion printhead with a 3-mL syringe and a 330-µm nozzle (23 Ga Metallic Orange needle).

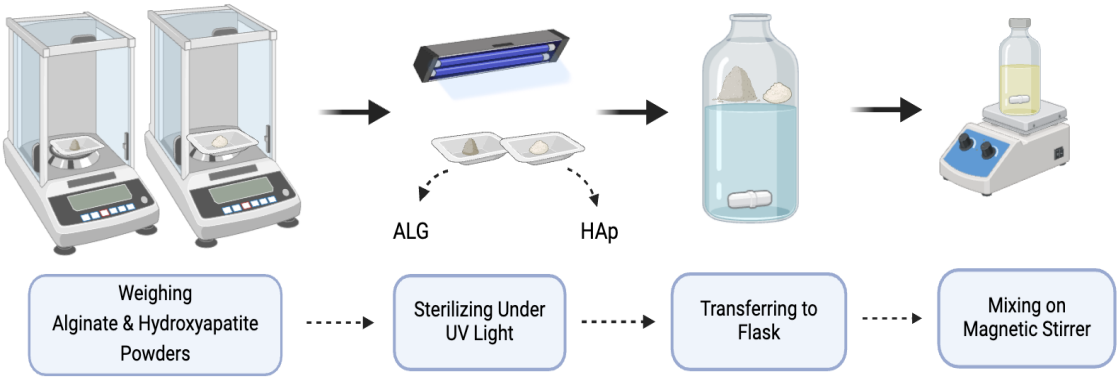

Figure 3.5 Preparation of sterile alginate and hydroxyapatite solutions (Designed with Biorender)

The 3D printing optimization work was started over the glass with the different HAp concentrations and with different parameters including pressure, speed, and number of layers. The results of these optimization trials, which maintained a constant 6 wt% alginate concentration while varying the hydroxyapatite concentrations, are summarized in **Table 3.3.**

Table 3.3 Optimization of 3D printing parameters for scaffolds with constant 6 wt% alginate and varying hydroxyapatite concentrations (N=3)

HAp (%, w/v) / Parameters	**%4**	**%4**	**%8**	**%8**	**%16**	**%16**	**%24**	**%24**
Speed (mm/s)	3	4	4	4	4	4	4	4
Pressure (bar)	0.5	1	1.5	2	4	5	6	8
Temperature (°C)	130	130	130	130	130	130	130	130
Number of Layers	5	5	5	5	5	5	5	5

Subsequently, *in situ* 3D printing was applied on the 3D head model, using the optimized parameters obtained from the various printing trials performed previously. Finally, 3D printed cylindrical scaffolds with dimensions of 8 x 8 x 5 mm were obtained. After the printing process, cross-linking of the bioink was achieved using a sterile 0.5 M $CaCl_2$ solution.

3.2.3.3 Mechanical Testing – Compression Test

The mechanical properties of the scaffolds were tested by the Universal Testing Machine (Shimadzu AGS-X, Japan) in the Laboratory of Biomechanics and Strength of Materials, Department of Biomedical Engineering, Ankara University. For the uniaxial compression test, scaffolds (n = 3) of dimensions 8 mm x 8 mm x 5 layers were loaded into the uniaxial compression testing machine with a 50N load cell and a test speed of 1 mm/min. The original length (L0) and the thickness were measured **(Figure 3.6)**. Then, the compression test was started, and the scaffolds were compressed at 1 mm/min compression speed until

sample failure was reached at room temperature. Stress−strain graphs were used to derive mechanical properties, including Young's modulus and ultimate compressive strength.

Young's modulus (YM) was reported as the slope of the stress-strain curve in the elastic region, and the ultimate compressive strength (UCS) values were determined as the maximum stress before failure, using the initial dimensions of the samples.

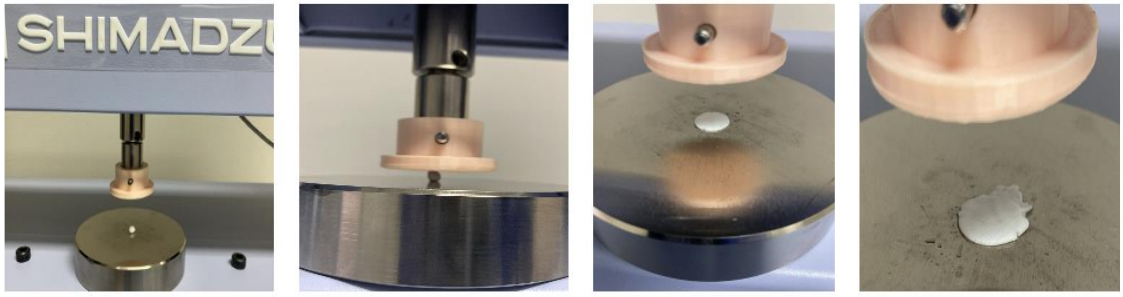

Figure 3.6 Application of uniaxial compression test to the Alg/HAp Scaffolds

3.2.4 Optimization of *in situ* 3D printing on the rabbit cadaver

The rabbit's cadaver was initially prepared for the *in situ* printing procedure. This preparation involved taking precise measurements of both the printer and the cadaver to facilitate the design of a custom stereotactic frame. These measurements were crucial for ensuring accurate alignment and positioning of the rabbit's head during the printing process. By accurately capturing the dimensions of the cadaver and the printer, the designed stereotactic frame ensured stability and precision, which are essential for the success of the 3D bioprinting process. This step was vital in achieving consistent and reproducible results, highlighting the importance of careful preparatory work in advanced bioprinting applications.

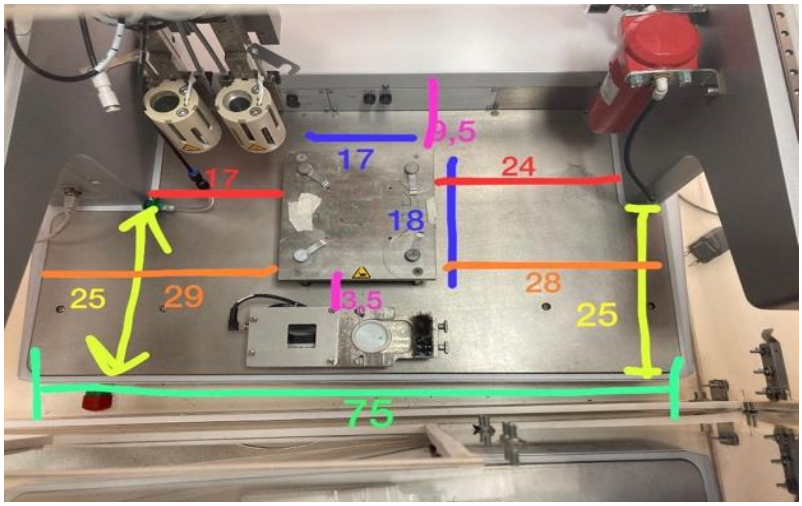

Figure 3.7 Measurements (in cm) of the 3D printer for designing the stereotactic frame

Subsequently, the cadaver was precisely placed on the printing platform, and the defect area was marked with a green circle to indicate the target region for printing. The height of the rabbit's head from the printing platform was measured to be approximately 6.8 cm. This measurement was used to set the substrate thickness (height) of the printer to 6.8 cm, ensuring proper calibration for the printing process.

Figure 3.8 Placement of the cadaver and marking of the defect area for *in situ* 3D printing

In situ 3D printing was applied directly onto the original size of the cadaver's head, with continuous optimization performed until the defect coverage was considered perfect. The head was securely fixed using stereotactic frames, which were custom 3D printed for this purpose. Printing was then initiated, utilizing a different pattern (Grid) for the scaffold to enhance structural integrity and conformity to the defect area.

3.2.5 Implementation of *in situ* 3D Printing on live rabbit models

3.2.5.1 Bioink preparation and sterilization with alginate and hydroxyapatite powders

The implementation of *in situ* 3D printing on live rabbit models began with the preparation of the bioinks, specifically with 6% (w/v) Alginate (Medium viscosity) and 8% (w/v) Hydroxyapatite (HAp) sterile mixture. The preparation was conducted under sterile conditions to ensure biocompatibility and prevent contamination.

Initially, the Hydroxyapatite and Alginate powders were sterilized separately by exposure to ultraviolet (UV) light for 30 minutes. Following sterilization, the powders were mixed with 1 mL of sterile PBS and 10 µL of penicillin/streptomycin (P/S) solution.

The resulting solutions were then subjected to vigorous agitation using a magnetic stirrer (Ika®, Germany) set to 500 rpm at room temperature (RT). This stirring process was maintained overnight to ensure thorough mixing and homogenization of the bioinks.
Simultaneously, a sterile solution of Calcium Chloride (0.5M $CaCl_2$) was prepared to serve as a crosslinking agent post-printing. This solution was essential for enhancing the structural integrity and stability of the printed constructs.

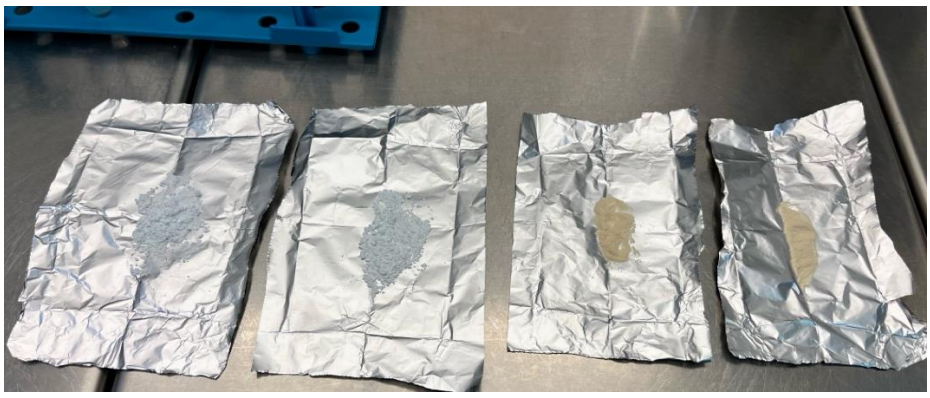

Figure 3.9 Sterilization of hydroxyapatite and alginate powders under UV light

3.2.5.2 Adipose-Derived stem/stromal cell isolation and culture

ASCs were isolated from rabbit subcutaneous adipose lipoaspirates. The cell isolation protocol was followed as described previously (Huri et al., 2018). Briefly, lipoaspirate was enzymatically digested by using 0.1% collagenase type I, 1% BSA, 2 mM $CaCl_2$ in PBS for 1h at 37°C. Samples were then centrifuged to isolate the stromal vascular fraction (SVF). Subsequently, the SVF pellet was plated onto tissue culture dishes to obtain the plastic-adherent population (P0). The adherent population (P0) was harvested upon confluence and stored in liquid nitrogen until use. ASCs were then thawed in expansion medium (Dulbecco's modified Eagle's medium (DMEM) supplemented with 10% fetal bovine serum (FBS), 1% penicillin/streptomycin (P/S), and 1 ng/mL FGF-2) under standard culture conditions (37 °C and 5% CO2). P1 ASCs were employed for the *in situ* bioprinting process over alive rabbits.

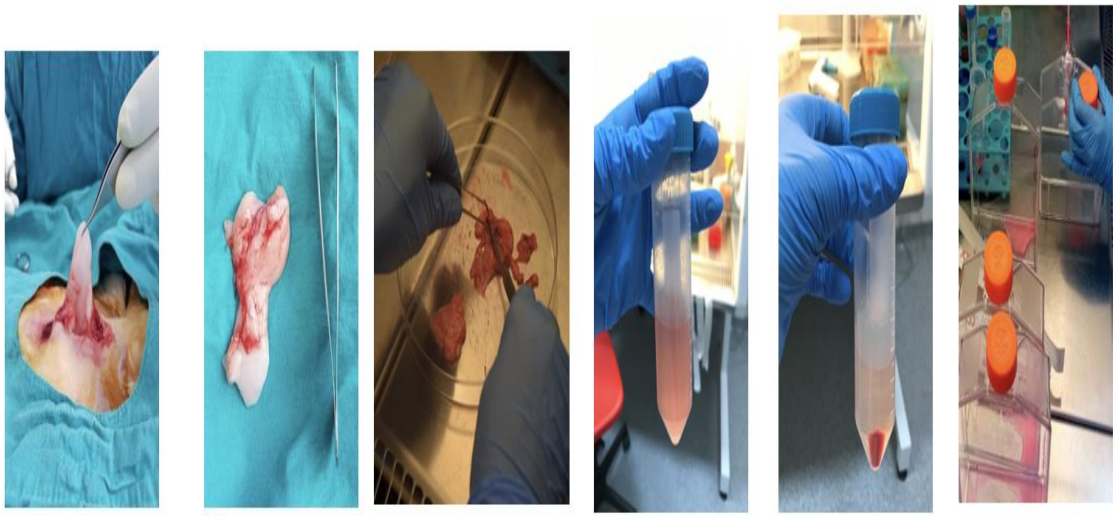

Figure 3.10 Isolation of Adipose-Derived Stem Cells (ASCs) for In Situ Bioprinting

3.2.5.3 In Situ bioprinting process over live animals

In situ 3D printing was performed on the rabbit craniofacial defects using % 6Alg / %8 HAp bioinks under sterile conditions. The %6 Alg / %8 HAp bioinks were loaded with 4.7×10^6 ASCs/mL and printed using 3D Bioplotter® (EnvisionTec, Germany) at room temperature (RT) using an extrusion printhead with a 3-mL syringe and a 330-μm nozzle

(23 Ga Metallic Orange needle). Finally, %6Alg / %8HAP scaffolds with dimensions of 8 x 8 x 5 mm and 5 layers were successfully printed over the alive animals, covering the whole defect area. Sterile 0.5 M $CaCl_2$ solution was added via micropipette to cross-link the bioinks prior to stitching.

3.2.6 Experimental animal procedures

All animal procedures were performed at the Animal Experiments and Research Lab of Medicine Faculty and MTELAB of Biomedical Engineering Faculty of Ankara University following a protocol approved by Ankara University Animal Research Ethics Committee (approval number 2022-3-26).

Eight healthy, male New Zealand white rabbits, 6 months of age with an average weight of 3.5 kg, were used for the study.

All rabbits were singly housed in standard stainless-steel cages, with ad libitum water and a standard commercial rabbit diet under the conditions of 55% humidity, room temperature (20-24°C), a 12-hour light cycle, and a 12-hour dark cycle.

In this study, the rabbits were categorized into three distinct experimental groups to assess the efficacy of different scaffold configurations in *in situ* 3D bioprinting for craniofacial bone regeneration. The experimental design was structured as follows:

- Group 1: Non-Cell-Seeded Scaffolds (n=6)
- Group 2: Cell-Seeded Scaffolds (n=6)
- Group 3: Empty Defect (Sham) (n=4)

This classification enabled a comprehensive evaluation of the efficiency of both cell-seeded and non-cell-seeded scaffold configurations in promoting bone regeneration through *in situ* bioprinting techniques.

3.2.6.1 Surgical operation

All interventional processes were carried out under sterile conditions and general anesthesia. Induction of general anesthesia was achieved by intramuscular administration of ketamine (35 mg/kg) in combination with xylazine (10 mg/kg). Maintenance of anesthesia was provided by total intravenous anesthesia (TIVA) with propofol at 0.5 mg/kg/min. The rabbits were intubated with a 3.0 mm cuffed endotracheal tube, and a purple-colored IV catheter was placed in the marginal vein of the ear. A balanced electrolyte solution was administered at 5 mL/kg/hr during anesthesia.

After clipping the skull hair and cleaning the area with alcohol and iodine solutions, eye lubricant was applied to both eyes. A pre-operative antibiotic, ceftriaxone at 50 mg/kg, was administered intramuscularly.

A 4 cm skin incision was made along the sagittal line on the top portion of the skull, and the periosteum was carefully faltered to expose the calvarium. Critical-sized circular defects with a diameter of 8 mm were created bilaterally on the parietal bone using a hand motor and round-tipped burr with continuous saline irrigation.

After the bioprinting process and the bioink filling the defects hardened, the periosteum, subcutaneous tissue, and incised skin were closed with a monofilament absorbable suture material (4/0 Polyglycolic acid) layer by layer in a simple continuous and simple interrupted pattern, respectively.

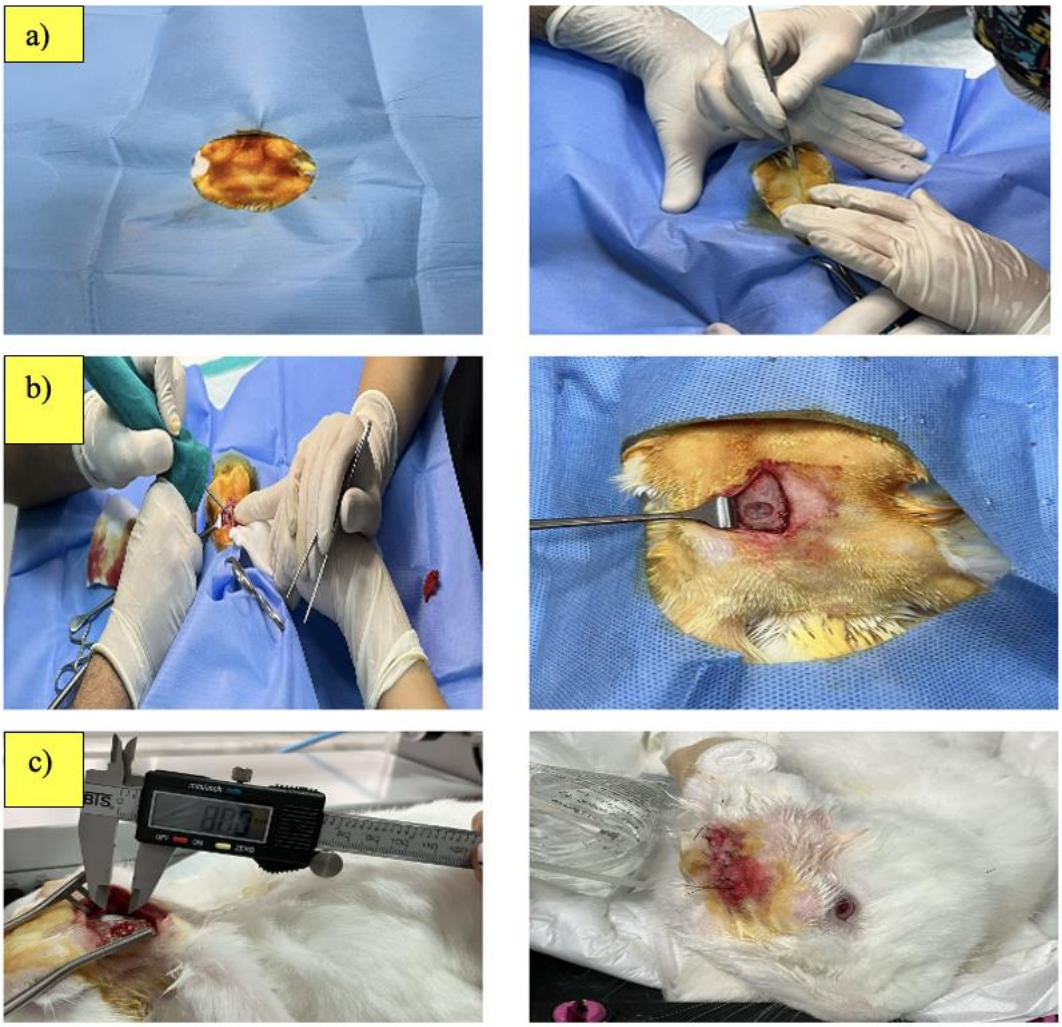

Figure 3.11 In situ 3D Bioprinting of Alg-HAp scaffolds within the rabbit cranium defect model. a-b) Defect creation and surgical exposure of the rabbit cranium, c) Defect coverage by bioprinting with its measurement, and post-printing stitching

3.2.7 Post-op analyses

Routine post-operative care followed surgery. Meloxicam (1 mg/kg) and ceftriaxone (50 mg/kg) were administered intramuscularly and continued for 72 hours post-op.

The animals were evaluated daily for wound healing progress, signs of pain or distress, and general activity. During the first, second-, and third-weeks post-surgery, one rabbit per week underwent computed tomography (CT) scanning to assess bone healing. At the

conclusion of the sixth post-operative week, euthanasia was performed using an overdose of intravenous sodium pentothal. Histopathological examination, and micro-computed tomography (micro-CT) were conducted on the relevant bone tissues.

3.2.7.1 Histopathological analysis

In this study, skulls from eight rabbits, divided into three different groups based on the material applied to the defect areas, were brought to the Department of Pathology at Ankara University Faculty of Veterinary Medicine. Histochemical examinations and evaluations of the provided samples were conducted.

The samples were fixed for 48 hours in neutral buffered formalin then decalcified in EDTA and hydrochloric acid solution (Biocal C, RRDC3-E, Atom Scientific LTD) for 3 days at 37℃ with daily solution replacement. They were dehydrated in a graded series of ethanol (70%-100%), cleared with xylene and subsequently embedded in paraffin.

Three serial 5 μm sections were collected from each sample and stained with hematoxylin and eosin (H&E, Merck) and Masson's trichrome (Beslab) staining technique for histopathological evaluation. Subsequently, the specimens were then examined under light microscope (Olympus BX51TF, Tokyo, Japan) in a blinded manner and recorded with an optical microscope (Olympus DP71, Tokyo, Japan).

3.2.7.2 Micro-CT scanning

A high-resolution, desktop Micro-CT system (Bruker Skyscan 1275, Kontich, Belgium) was used to scan the specimens. The scanning conditions were: 80 kVp, 125 mA, with 1 mm Al filter, 25 μm pixel size. To minimize artifacts, flat field correction of the detector was carried out. Each sample was scanned with 360˚ through rotation at 0.2 step. The mean time of scanning was around 30 min.

Figure 3.12 Micro-CT scanning process

The NRecon software (ver. 1.7.4.2, Bruker Skyscan, Kontich, Belgium), which used the modified algorithm described by Feldkamp et al. to obtain axial, two- dimensional (2D) images. The reconstruction parameters were used as ring artifact correction was set to 7, smoothing was 3 and the beam artifact correction was set at 38%. Image conversion limits were used as 0.0-0.04 for all the samples. NRecon the images obtained by the scanner were reconstructed to show 2D slices of the specimen. CTAn (ver. 1.23.0.2+, Bruker Skyscan, Kontich, Belgium) was used for the quantitative 3D and 2D measurements of the samples.

After reconstruction, region of interests (ROI) were drawn to include the 3D printed material within the sample using CTAn software, which all specifications of the program was used in order to analyze the 3D microarchitecture of newly formed bone tissue.

To analyze the newly format tissues, global thresholding was used for all the samples and the limits of the threshold were 50-255 (in gray scale values), the upper limit was at the top end of the brightness spectrum representing the highest bone density value. After thresholding (binarization) process, an imposed image of black/white pixels only achieved. Then, separately for each slice, a region of interest was chosen to contain 3D printed material to allow calculation of new bone tissue.

Also, for the determination of the Bone Mineral Density (BMD) Hydroxyapatite calibration blocks with density of 0.25 g/cm^3 and 0.75 g/cm^3 used to determine the calibration. The calibration curve was used to determine the BMD values of the samples. CTVox (ver. 3.3.0 r1403, Bruker Skyscan, Kontich, Belgium) was used for the visualization of the samples in 3D.

All specifications of the program were used in order to analyze the 2D and 3D microarchitecture of each sample. The following structural parameters were measured; percent object volume, object surface /volume ratio, object surface density, structure model index, structure thickness, structure linear density, structure separation, connectivity, connectivity density. Those parameters were calculated three dimensionally (3D) based on the volume of the ROI.

3.3 Statistical Analysis

Statistical analyses were performed using GraphPad Prism (version 10) software. Statistical differences were determined by analysis of variance (ANOVA) followed by Tukey's multiple comparison test or Student's *t*-test where appropriate. Numerical and graphical results are displayed as mean ± standard deviation. Significance was accepted at a level of $p < 0.05$. Sample size (n) is indicated within the corresponding figure legends.

4. RESULTS AND DISCUSSION

4.1 Optimization of *in Situ* 3D Printing

The optimization trials were conducted on the models listed below, and notably, defect No. 9 was completely covered through *in situ* 3D printing using the optimal parameters specified in **Table 4.1**.

Table 4.1 Optimization parameters for ın situ 3D bioprinting using PCL material *(The table details the parameters used in the optimization trials, with the optimal parameters for defect No. 9 highlighted in bold.)*

Parameters						
Speed (mm/s)	3	3	3	2.5	2.5	**2.5**
Pressure (bar)	5.5	5.5	5.5	5.5	4.5	**4.5**
Temperature (°C)	130	130	130	130	130	**130**
Waiting Time (sec)	30	20	10	10	10	**0**
Result; Fail/Success (F/S)	F	F	F	F	F	**S**

The **Figure 4.1** illustrates the printing results, showing the successful coverage of defect No. 9 with high precision.

Figure 4.1 In situ 3D bioprinting results and defect coverage in the small models of the rabbit cranium

Consequently, *in situ* 3D printing was applied directly onto the printed head model using the optimized parameters **(Figure 4.2)**. The defect coverage was achieved with a high degree of precision. This successful application underscored the efficacy of the methodology and the potential of *in situ* 3D printing. Consequently, it was decided to initiate the process by preparing the appropriate bioink and printing it over the printed head model, employing alginate as a primary material.

Figure 4.2 In situ 3D bioprinting results and defect coverage in rabbit cranium model

4.2 Printing Optimization of Alginate

The *in situ* 3D printing process was successfully optimized for printing alginate-based bioinks on the 3D head model. The optimization involved systematic trials varying key parameters, including alginate concentration (6%, 8%, and 10%), extrusion pressure, speed, and temperature. The data from these trials were compiled into a comprehensive table **(Table 4.2)**, which revealed that the 6% alginate concentration provided the best results under specific conditions.

Table 4.2 Optimization parameters for *in situ* 3D bioprinting using alginate material. *(This table presents the parameters for different alginate concentrations, with 6% concentration highlighted as optimal.)*

Alginate (%, w/v) / Parameters	**%6**	**%6**	**%6**	**%8**	**%8**	**%8**	**%10**	**%10**	**%10**
Speed (mm/s)	3	3	**3**	3	3	3	3	2	2
Pressure (bar)	3	2	**1.5**	2	2.5	3	3.5	3.5	4
Temperature (°C)	30	30	**30**	30	30	30	30	30	30
Result (F/S)	F	F	**S**	F	F	F	F	F	F

The 6% alginate concentration, when printed with the optimized parameters for pressure, speed, and temperature, and Fail/Success (F/S) demonstrated the greatest accuracy in covering defects and overall print quality. The 8% alginate concentration showed improved mechanical stability and the same print accuracy but was less effective than the 6% concentration under the same conditions. The 10% alginate concentration, while providing the highest mechanical strength, was challenging to extrude due to its high viscosity, resulting in frequent nozzle clogging and lower print accuracy. Inks below or above this alginate concentration range were discarded due to the non-homogeneous appearance obtained for the 3D-printed hydrogels, and the 6% alginate was considered the best concentration to be used.

After printing, the 3D printed alginate cylindrical scaffolds with dimensions of 8 x 8 x 5 mm were cross-linked using a sterile 0.5 M $CaCl_2$ solution. Although SEM analysis and additional tests were not conducted in this study, findings from related literature indicate that the 6% alginate concentration supports favorable outcomes in terms of cell viability, cell attachment, and cell migration (Iglesias-Mejuto & García-González, 2021).

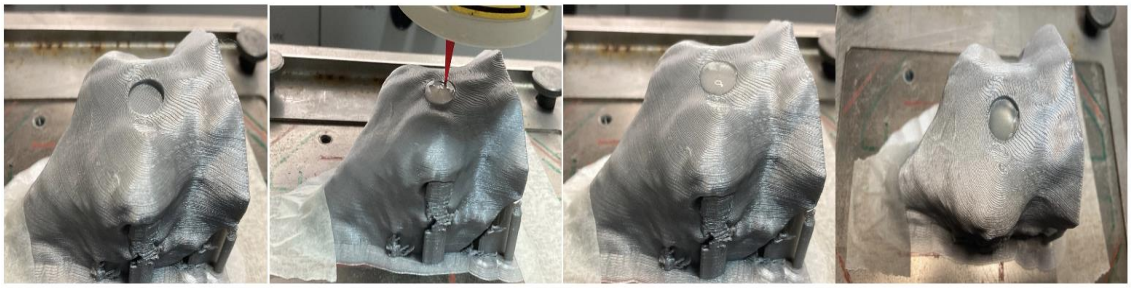

Figure 4.3 In situ 3D bioprinting results showing complete defect coverage in rabbit head model with 6% alginate

4.3 Printing Optimization of Alginate & Hydroxyapatite

The optimization of 3D printing using alginate and hydroxyapatite (HAp) was successfully achieved, where scaffolds with varying HAp concentrations (4, 8, 16, and 24 wt%) combined with 6 wt% alginate were fabricated. The solutions were prepared through vigorous agitation and subsequently printed using the 3D Bioplotter® (EnvisionTec, Germany) under optimized conditions.

The 3D printing optimization was conducted first on glass slides with varying parameters, including extrusion pressure, printing speed, and layer number **(Figure 4.4)**. The results demonstrated that lower pressures resulted in less consistent filament formation, while higher pressures increased the risk of clogging. Ultimately, the optimized parameters for printing the 6% alginate and 8% HAp combination allowed for the successful fabrication of cylindrical scaffolds with dimensions of 8 x 8 x 5 mm.

Figure 4.4 Cylindrical scaffolds with various concentrations of HAp printed on glass slides using different printing parameters

Initial trials indicated that the addition of HAp significantly affected the printability and structural integrity of the resulting scaffolds. Among the tested concentrations, the combination of 6 wt% alginate with 8 wt% HAp yielded the best results in terms of print quality and scaffold stability. This optimal formulation provided a balanced viscosity that facilitated smooth extrusion and maintained the desired shape during the printing process on the head model as well **(Figure 4.5)**.

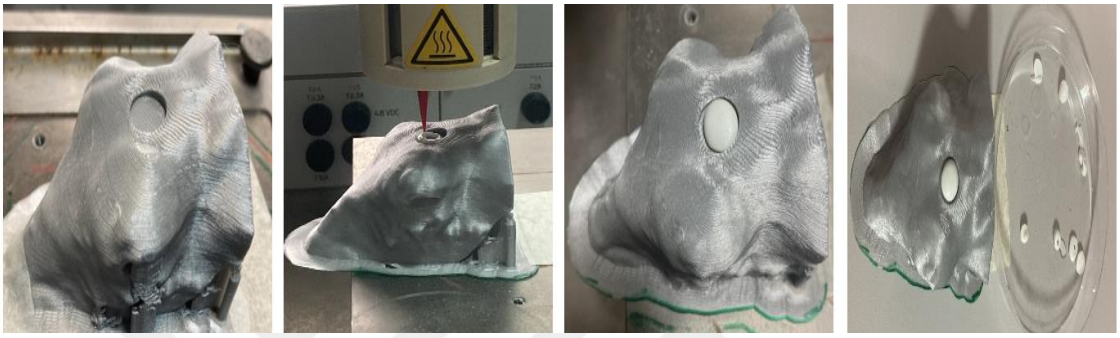

Figure 4.5 Scaffolds of 6 wt% Alginate with 8 wt% HAp printed on rabbit head model using optimized printing parameters

After the printing process, scaffolds underwent cross-linking using a sterile 0.5 M $CaCl_2$ solution, enhancing their mechanical properties. Although SEM analysis and additional tests were not performed in this study, existing literature indicates that the incorporation of HAp into alginate-based scaffolds supports enhanced osteogenic potential and promotes bone formation (Iglesias-Mejuto & García-González, 2021).

The resulting scaffolds displayed excellent structural integrity and homogeneity, with images included in the results section demonstrating the successful printing over both the glass substrate and the 3D head model. Additionally, the graph in **Figure 4.6** illustrates the printability trials of scaffolds with various concentrations of HAp. It confirms that the 8% HAp and 6% alginate combination demonstrates superior printability compared to other concentrations.

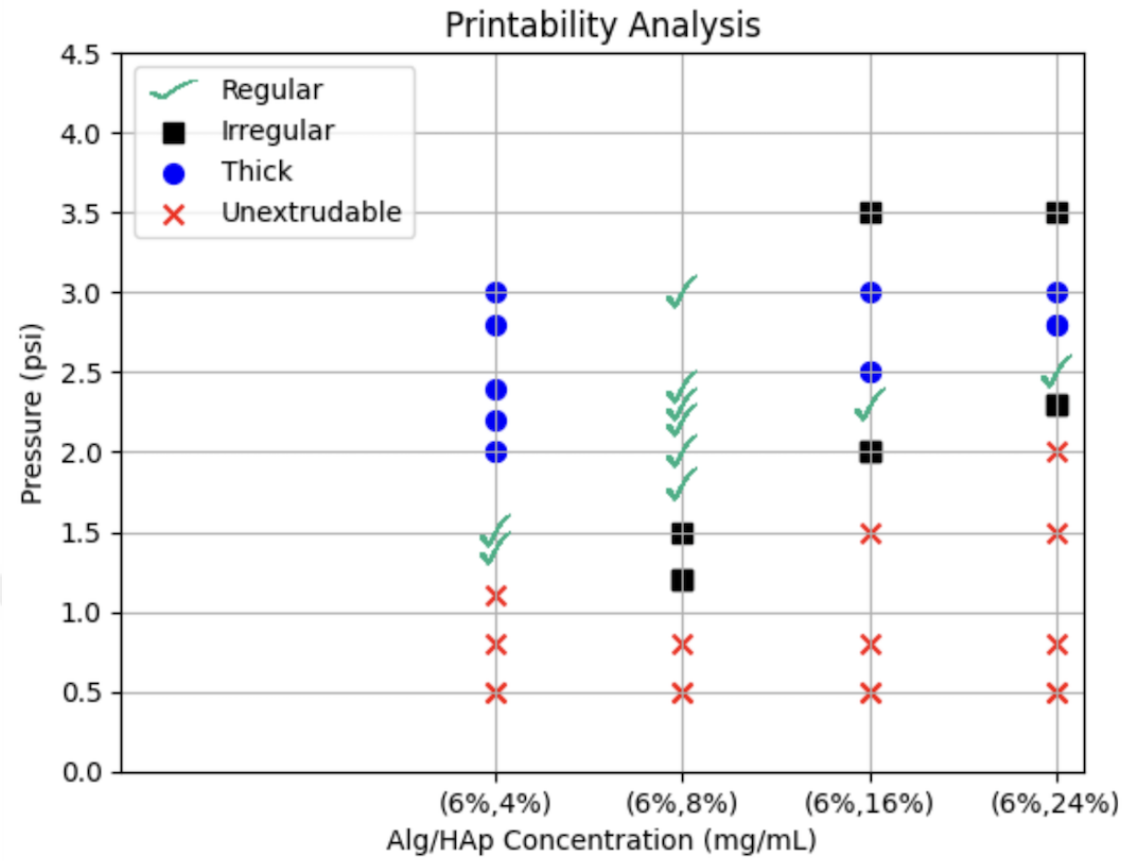

Figure 4.6 Printability analysis of scaffolds with various HAp concentrations (4, 8, 16, and 24 wt%) combined with 6 wt% alginate, showing line models for different printing parameters

4.4 Mechanical Properties of the Bioinks

Stress-strain graphs were utilized to obtain the mechanical properties, specifically Young's modulus (YM) and ultimate compressive strength (UCS). Young's modulus is defined as the ratio of stress to strain in the elastic region of the material, providing information about the stiffness and elasticity of the scaffold. For alginate scaffolds, YM was found to be 0.023 ± 0.03 MPa, indicating a relatively low stiffness suitable for applications requiring higher elasticity. UCS, defined as the maximum stress the material can resist before failure, was measured at 0.059 ± 0.005 MPa for alginate scaffolds. In contrast, the scaffolds composed of alginate and hydroxyapatite (Alg/HAp) exhibited a YM of 0.030 ± 0.15 MPa, which, although slightly higher, still suggested a degree of elasticity conducive to bone tissue engineering. The UCS of Alg/HAp

scaffolds was significantly higher at 0.394 ± 0.04 MPa, indicating a considerable improvement in mechanical strength due to the addition of hydroxyapatite.

These results, summarized in **Table 4.3**, demonstrate that while both alginate and Alg/HAp scaffolds possess suitable mechanical properties for bone regeneration, the addition of hydroxyapatite enhances the mechanical strength significantly. The increase in UCS with the addition of hydroxyapatite underscores the potential of these composite scaffolds to provide the necessary mechanical support for bone regeneration.

This improvement in mechanical strength is critical for supporting bone tissue, which undergoes significant mechanical loading during physiological activities. Additionally, hydroxyapatite contributes to the osteoconductivity of the scaffold, facilitating better cell attachment, proliferation, and differentiation. The increased mechanical strength of Alg/HAp scaffolds aligns with the requirements for effective bone regeneration, providing a more supportive environment for new bone growth.

Table 4.3 Mechanical Properties of Alginate and Alginate/Hydroxyapatite Scaffolds

	Young's Modulus (MPa)	Ultimate Compressive Strength (MPa)
Alginate	0.023 (± 0.03)	0.059 (± 0.005)
Alginate/Hydroxyapatite	0.030 (± 0.15)	0.394 (± 0.04)

4.5 In Situ 3D Printing on Rabbit Cadaver

The *in situ* 3D printing procedure was successfully applied to a rabbit cadaver, following the optimization of printing parameters with alginate and hydroxyapatite (Alg/HAp) bioink. The rabbit cadaver was initially prepared by taking precise

measurements of both the printer and the cadaver to design an appropriate stereotactic frame. This ensured accurate alignment and positioning of the rabbit's head during the printing process. The defect area on the cadaver was clearly marked, and the height of the rabbit's head from the printing platform was measured to be approximately 6.8 cm. This measurement was utilized to set the substrate thickness (height) of the printer, ensuring proper calibration for the printing process.

The cadaver was then securely placed on the printing platform, and the *in situ* 3D printing was executed directly onto the defect area of the rabbit's head. Continuous optimization of the printing parameters was performed until the defect coverage was deemed satisfactory. The head was immobilized using custom 3D-printed stereotactic frames to maintain stability during the printing procedure. A grid pattern was employed for the scaffold to enhance structural integrity and better conform to the defect area.

The printing results on the cadaver were highly satisfactory, with the defect being completely covered by the Alg/HAp bioink. Initial grid lines of the scaffold were clearly visible in the first layers of the print **(Figure 4.7)**. However, due to the crosslinking effect and the uneven surface of the skull, these grid lines were not as apparent in the upper layers of the scaffold. Despite this, the final layers achieved complete defect coverage, demonstrating the effectiveness of the optimized *in situ* printing strategy.

Figure 4.7 Initial grid lines of the scaffold visible in the first layers and the final layer (after crosslinking) achieving complete defect coverage

Following the successful implementation of the printing procedure on cadaver, the subsequent phase involves transitioning to *in situ* 3D printing on live rabbit models.

4.6 In Situ 3D Printing on Live Rabbit Models

Following the successful application of *in situ* 3D printing on cadaver models, the procedure was translated to live rabbit models. This advancement aims to further validate and evaluate the effectiveness of the optimized printing strategy within a living biological system. The *in situ* 3D printing was carried out on craniofacial defects of live rabbits using 6% Alginate / 8% Hydroxyapatite (Alg/HAp) bioinks. The bioinks, loaded with 4.7 $\times 10^6$ adipose-derived stem cells (ASCs)/mL, were printed at room temperature using the 3D Bioplotter® (EnvisionTec, Germany). **Table 4.4** below summarizes the coverage efficiency and printing accuracy achieved during the experiments. The data demonstrates a high level of precision in scaffold placement and defect coverage.

Table 4.4 Quantitative data on *in situ* 3D bioprinting on live rabbit models

Parameter	**Value (Mean ± SD)**	**Description**
Scaffold Dimensions	8 x 8 x 5 mm	Length, width, and height of the scaffold
Layer Thickness	0.33 ± 0.05 mm	Thickness of each printed layer
Coverage Area	64 mm²	Total area covered by the scaffold
Printing Time	8 ± 2 minutes	Time taken to print each scaffold
Coverage Efficiency	100%	Percentage of defect area covered
Printing Accuracy	95% ± 3%	Accuracy of scaffold placement
Initial Grid Visibility	High (first 3 layers)	Visibility of grid lines in initial layers
Final Layer Integration	Complete	Integration and coverage in final layer

The printing results demonstrated that the Alg/HAp bioink successfully covered the entire defect area in all live animals. The scaffolds, with dimensions of 8 x 8 x 5 mm and comprising 5 layers, adhered well to the defect sites and provided complete coverage. Despite the challenges of working with live tissue, the printed scaffolds maintained their

structural integrity and conformed well to the defect areas. **Figure 4.8** shows the scaffold immediately after printing and following cross-linking with CaCl2 solution.

Figure 4.8 The in situ 3D bioprinting process a) Defect Creation, b,c) Scaffold coverage and structural integrity post-printing, d) cross-linking in live rabbit models

The successful coverage and integration of the bioink in live animals further validated the efficacy of the optimized *in situ* 3D printing parameters for craniofacial bone regeneration. This step marks significant progress in the application of bioprinting techniques for in vivo bone tissue engineering.

Overall, the successful application of the optimized *in situ* 3D printing strategy on live rabbit models demonstrates its potential for effective bone regeneration. The next phase of the study will focus on evaluating the long-term outcomes and integration of the printed scaffolds in living systems.

4.7 Histopathological Analysis

The histopathological analysis of craniofacial defect samples from the rabbit models revealed significant differences between the various groups. In defects filled with acellular material, a thin capsule structure was observed around the material, primarily consisting of fibrocytes (**Figure 4.9)**. Mononuclear cell infiltrations, predominantly lymphocytes, were noted on and around the capsule, accompanied by the formation of a few new blood vessels. Additionally, periosteal proliferations were seen extending into

and around the material, indicating a response to the implanted scaffold (**Figure 4.10, Figure 4.11)**.

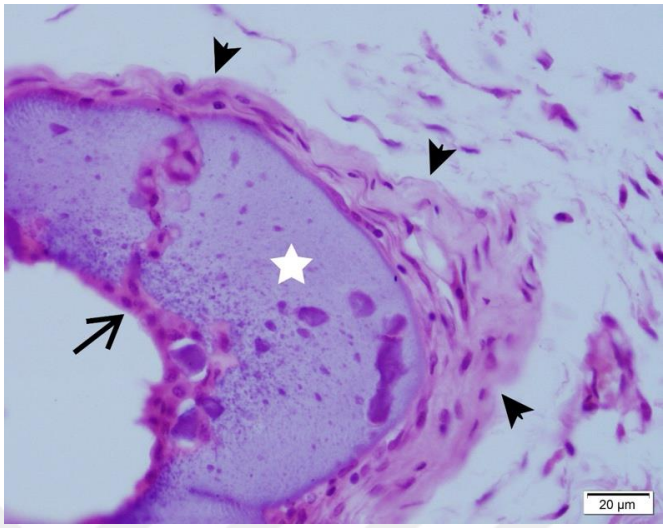

Figure 4.9 Acellular material (white star), periosteal proliferations (arrow), fibrous capsule (arrowheads)

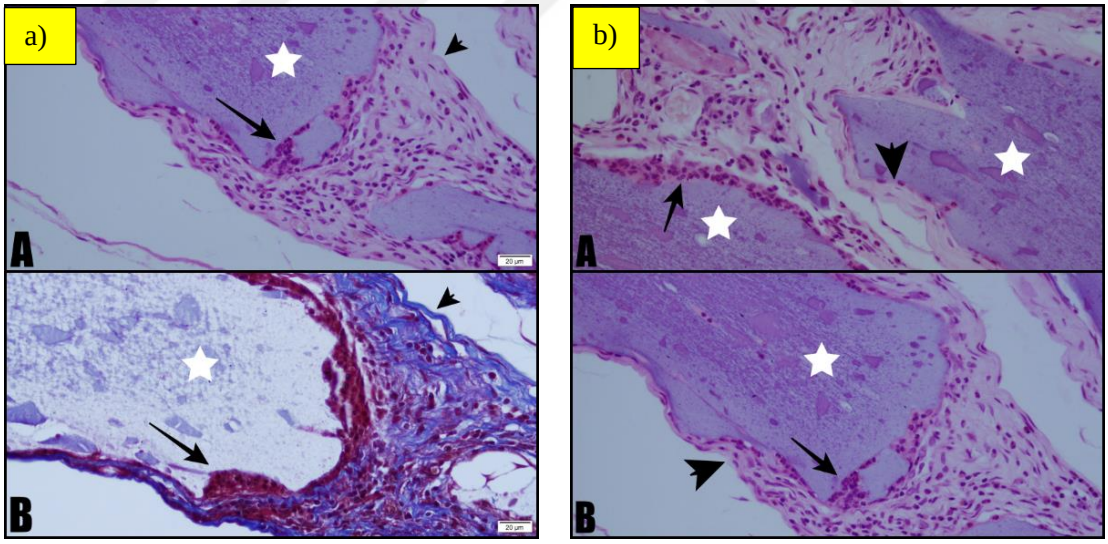

Figure 4.10 a) A: HxE, B: Trichrome staining. Acellular material (white star), periosteal proliferations (arrow), fibrous capsule (arrowheads), b) A, B: HxE staining. Acellular material (white star), periosteal proliferations (arrow), fibrous capsule (arrowheads).

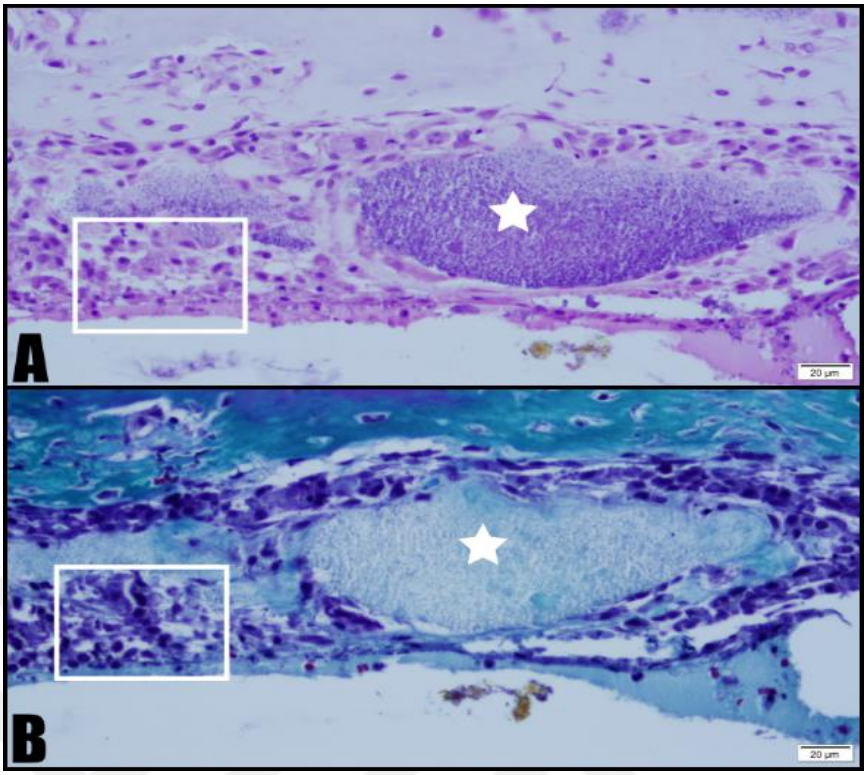

Figure 4.11 A: HxE, B: Trichrome staining. Acellular material (white star), mild mononuclear cell infiltration (square)

In contrast, defects filled with cellular material exhibited a thicker capsule structure, primarily composed of fibroblasts and collagen fibers. This group showed numerous segmented and/or pyknotic neutrophils on the capsule and severe inflammatory cell infiltration immediately outside the capsule, consisting of lymphocytes, plasma cells, and a few macrophages (**Figure 4.12, Figure 4.13)**. The presence of many newly formed blood vessels was also noted. Large, vesicular, round nuclei with broad eosinophilic cytoplasmic cells, likely osteoblasts, were found near the material, suggesting active bone formation. A wide ring of mononuclear cell infiltrations and multinucleated cells was observed around one of the cellular materials, indicating a robust inflammatory and regenerative response (**Figure 4.14, Figure 4.15)**

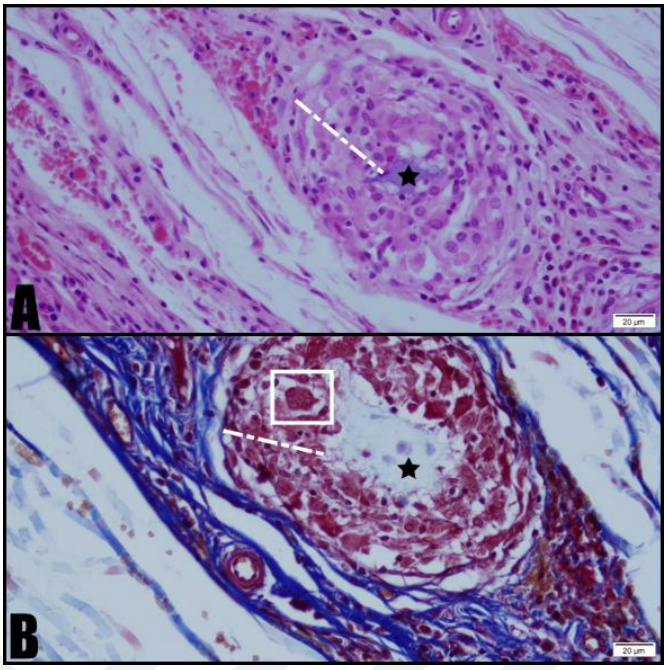

Figure 4.12 A: HxE, B: Trichrome staining. Cellular material (black star), mononuclear cell infiltration (dashed line), multinucleated cell (white square)

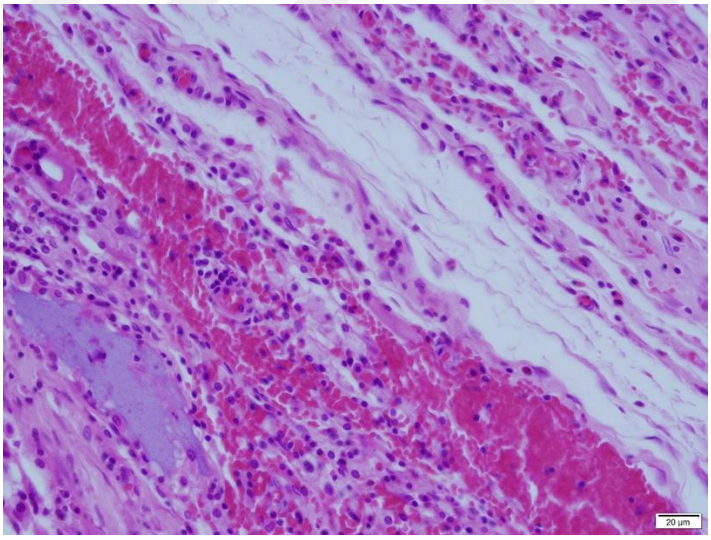

Figure 4.13 Dense free erythrocyte accumulations around cellular material

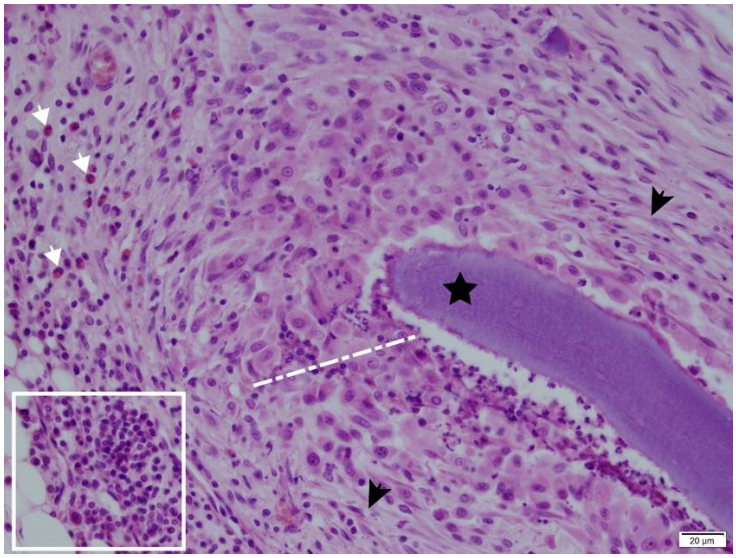

Figure 4.14 Cellular material (black star) with neutrophil and mononuclear cell infiltrations (dashed line/square), thin connective tissue (arrowhead), and eosinophil infiltration (white arrowhead)

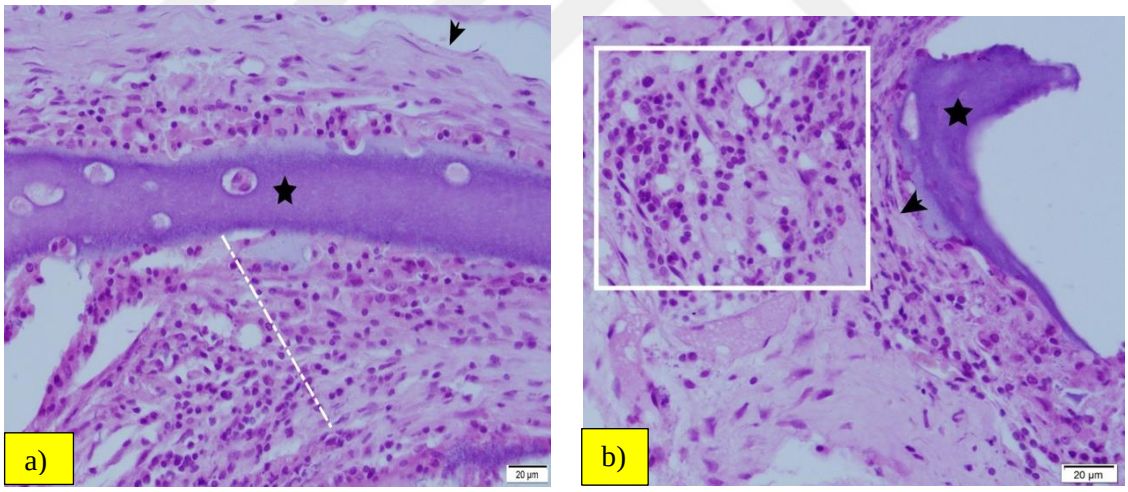

Figure 4.15 a) Cellular material (black star) with mononuclear cell infiltrations (dashed line) and thin connective tissue (arrowhead), b) Cellular material (black star) with mononuclear cell infiltrations (dashed line/square) and thin connective tissue (arrowhead)

In the empty defects, adipose tissue and thick trabeculae formed by connective tissue, primarily fibrocytes and collagen fibers, were observed, suggesting an attempt at repair rather than true bone regeneration (**Figure 4.16)**. The adipose tissue and connective tissue

increase in these defects likely aim at stabilizing the area, potentially forming scar tissue in the long term.

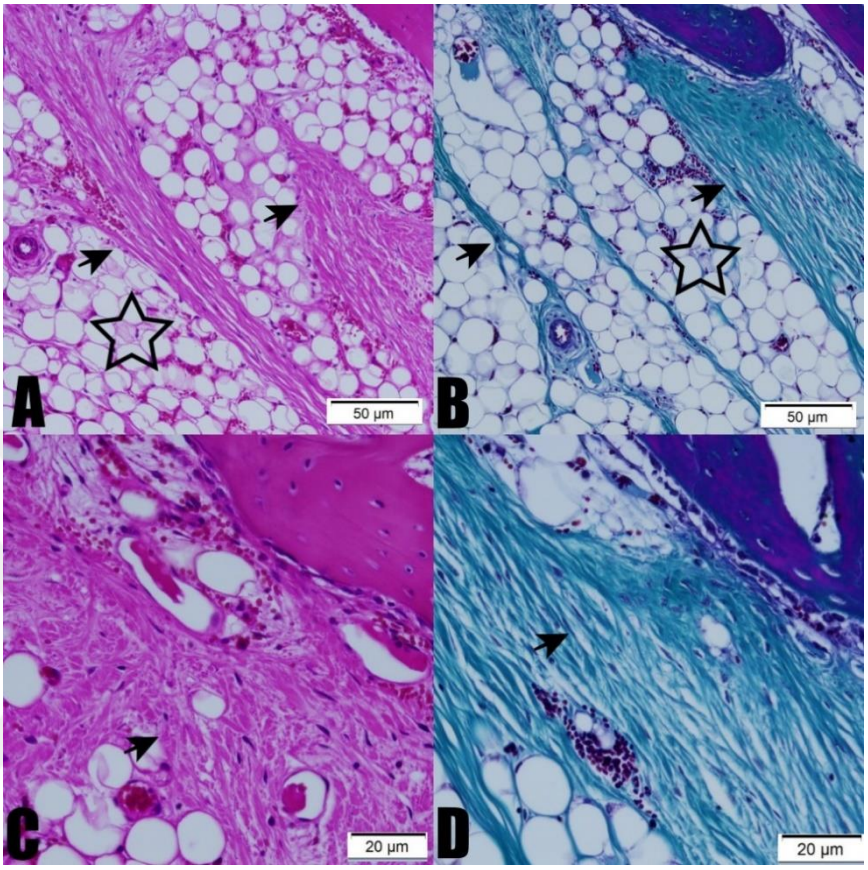

Figure 4.16 A, C: HxE; B, D: Trichrome staining. Adipose tissue (empty black star) and connective tissue (arrowhead) filling the empty defect

The histopathological findings highlight the different responses elicited by acellular and cellular scaffolds. The collagen-dominant capsule formation in the group with cellular material indicates a delayed fibrosis (scar formation). The increased inflammation and neovascularization in the group with cellular material compared to the group with acellular material suggest a prolonged inflammatory period, allowing for more effective tissue repair before fibrosis occurs. Healing was more pronounced in defects filled with both types of materials compared to empty defects, indicating the potential of these scaffolds for effective bone regeneration. However, the empty defects were predominantly filled with adipose tissue, accompanied by significant connective tissue increase, which might form scar tissue in the long term. Repeating a similar study at

different durations to observe long-term results would provide more detailed and accurate information about the outcomes of these scaffolds.

4.8 Micro CT Scanning Results

The *in situ* 3D bioprinting experiments were conducted to evaluate the effectiveness of Alg/HAp scaffolds in craniofacial bone regeneration in a live rabbit model. This study involved three groups: non-cell-seeded, cell-seeded, and sham group (control). Each group was assessed to determine the efficacy of the bioprinted scaffolds in promoting bone regeneration and healing of craniofacial defects. Key parameters such as bone volume, bone surface density, and structural properties were measured using CT imaging to provide a comprehensive analysis of the scaffold performance.

Detailed observations were made for each rabbit, focusing on defect coverage and bone formation. The results were compared across the groups to determine the relative effectiveness of the cell-seeded and non-cell-seeded scaffolds in contrast to the sham group. The detailed results below, including quantitative measurements and qualitative observations, highlights the success and challenges encountered during the *in situ* bioprinting process. This comprehensive evaluation aims to provide insights into the potential of Alg/HAp scaffolds for clinical applications in bone tissue engineering.

The non-cell-seeded group showed hopeful results. For instance, in the second rabbit (2R and 2L), both defects were completely covered. However, the defect at 2L showed some bone particles, likely remnants from the drilling process that were not adequately cleaned and went under the skin. The average bone volume for all non-cell-seeded defects was 27.2 mm^3.

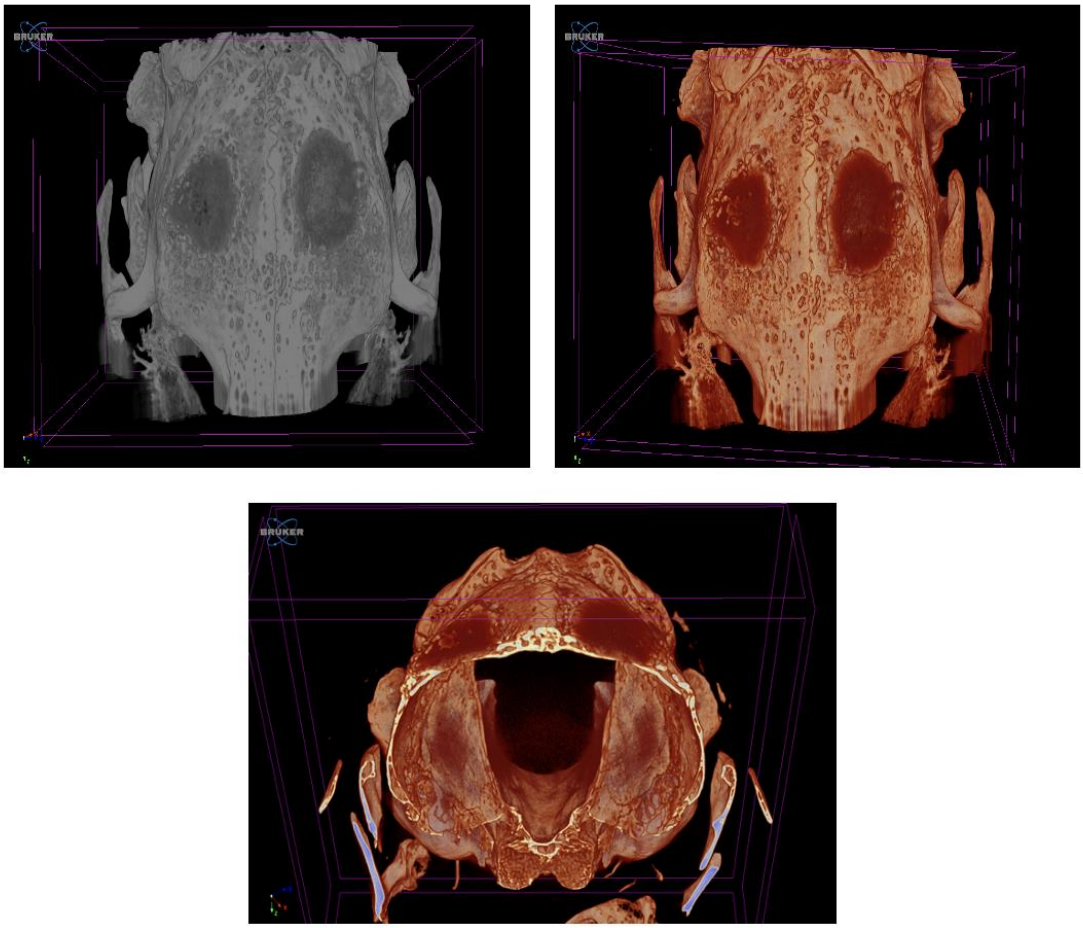

Figure 4.17 CT images of defects 2R and 2L in the second rabbit (Non-Cell-Seeded Group)

The cell-seeded group exhibited promising outcomes, where the fourth rabbit (4R and 4L), for instance, displayed not only complete defect coverage but also significant bone formation. The average bone volume for all cell-seeded defects was 32 mm^3, which was higher than that of the non-cell-seeded group.

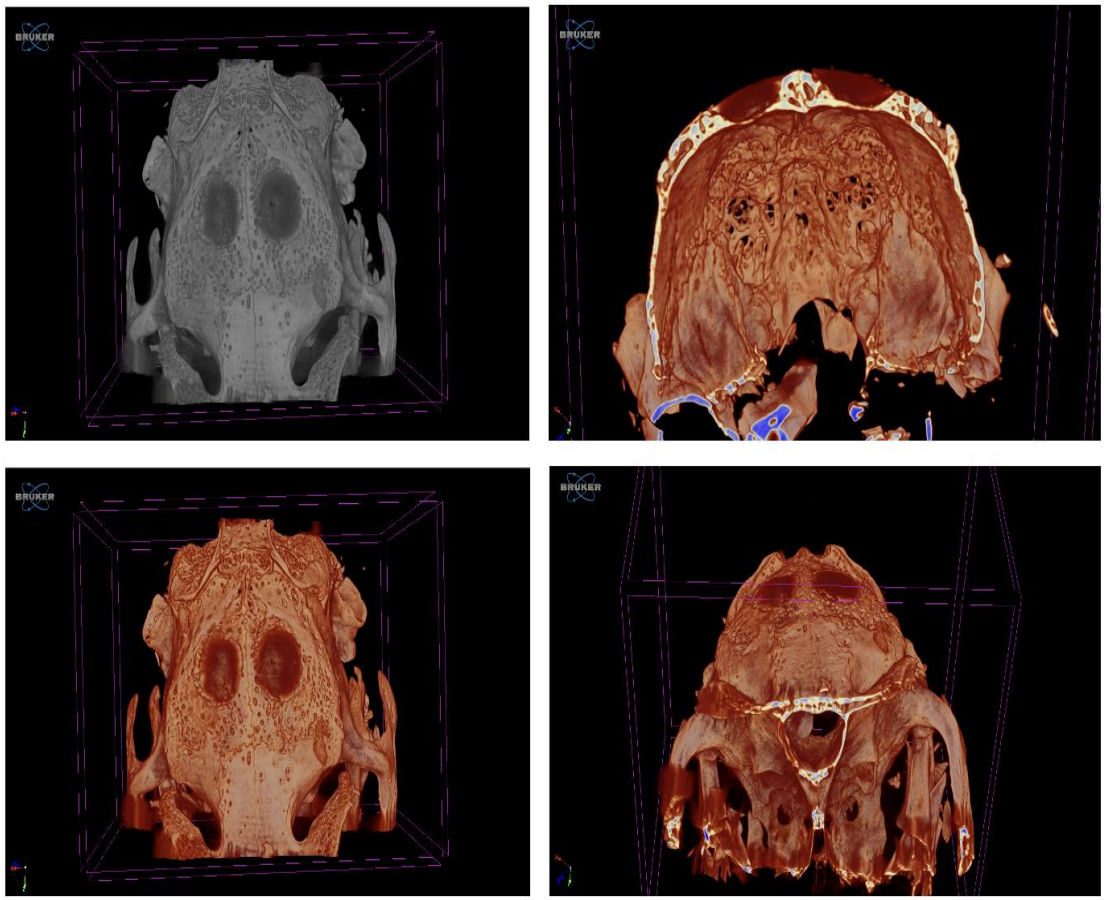

Figure 4.18 CT images of defects 4R and 4L in the fourth rabbit (Cell-Seeded Group)

By comparing the cell-seeded and control defects, rabbit 5, had one cell-seeded defect (5L) and one control defect (5R). The 5L defect showed excellent defect coverage and substantial bone formation, with a bone volume of 50.7 mm^3. In contrast, the control defect 5R, which was left empty, had a bone volume of only 0.27 mm^3. This indicates that the bioprinted Alg/HAp material significantly promotes bone regeneration and formation.

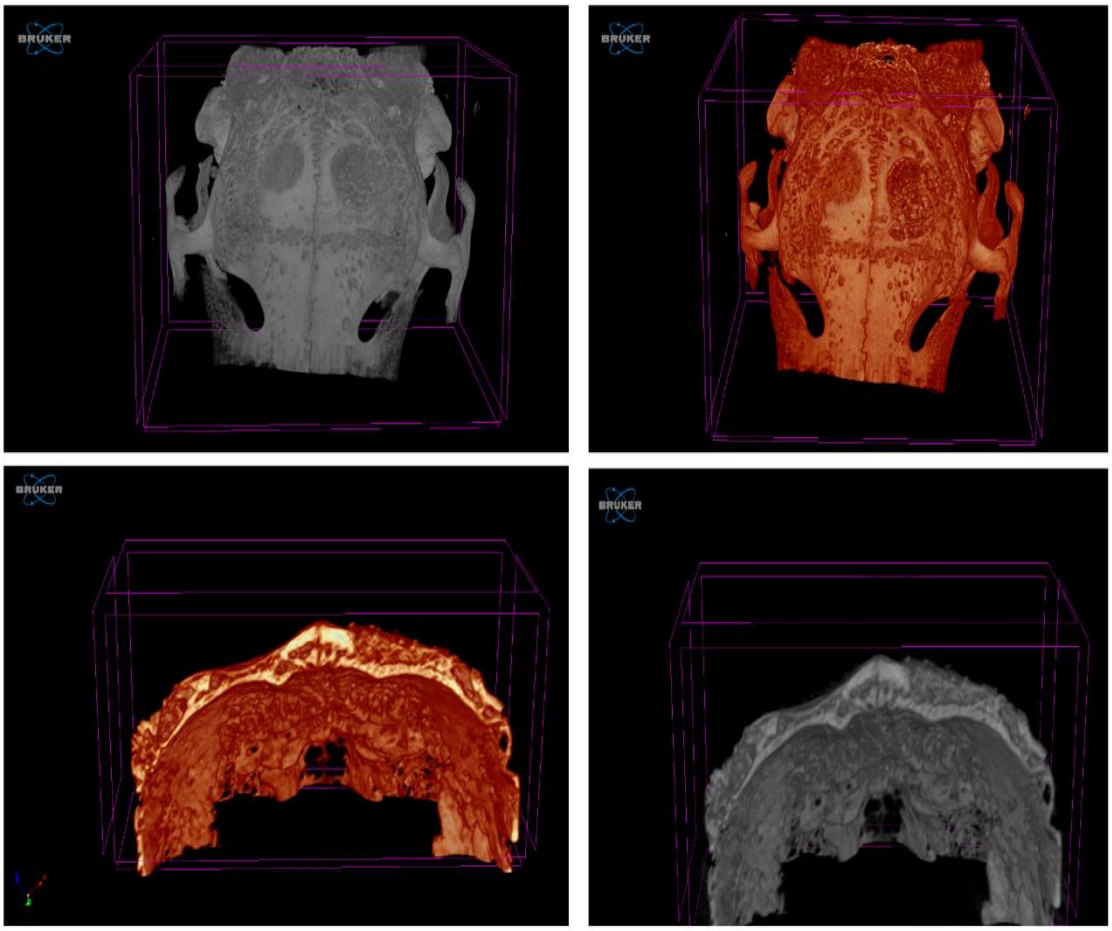

Figure 4.19 CT images of Cell-Seeded Defect (5L) and Control Defect (5R) in Rabbit 5

However, by comparing the cell-seeded and control defects, rabbit 7 had one non-cell-seeded defect (7L) and one control defect (7R). The 7L defect exhibited good defect coverage and bone formation, with a bone volume of 32.12 mm^3. The control defect 7R had a bone volume of 0.35 mm^3, highlighting the effectiveness of the bioprinted Alg/HAp material without cells. However, the cell-seeded defect in 5L showed better results in bone formation and volume compared to the non-cell-seeded defect.

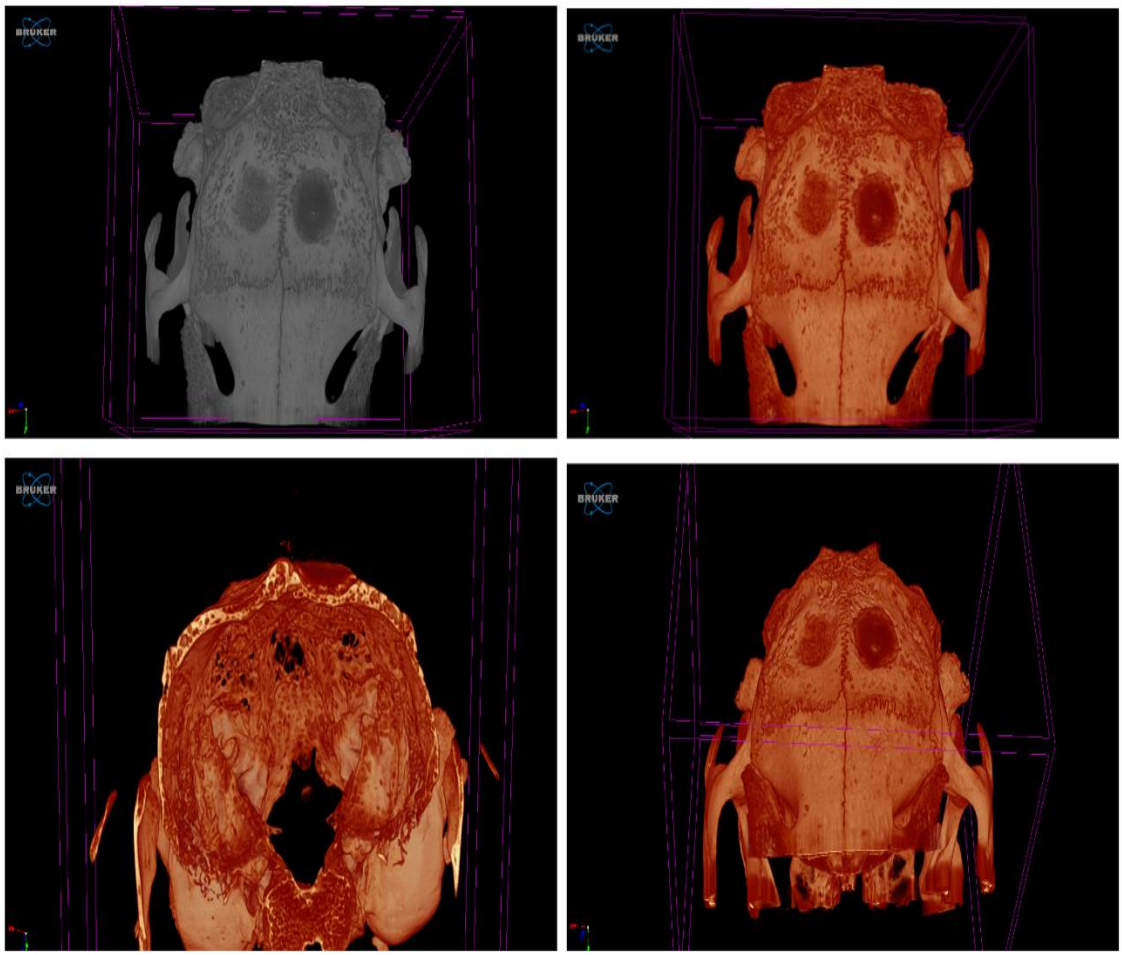

Figure 4.20 CT Images of Non-Cell-Seeded Defect (7L) and Control Defect (7R) in Rabbit 7

Moreover, by comparing the non-cell-seeded and cell-seeded defects, rabbit 6 had one non-cell-seeded defect (6L) and one cell-seeded defect (6R). Both defects demonstrated great defect coverage and bone formation. However, the 6R defect, which was cell-seeded, showed slightly higher bone formation, as indicated by the brighter orange color at the borders of the defect in the CT images.

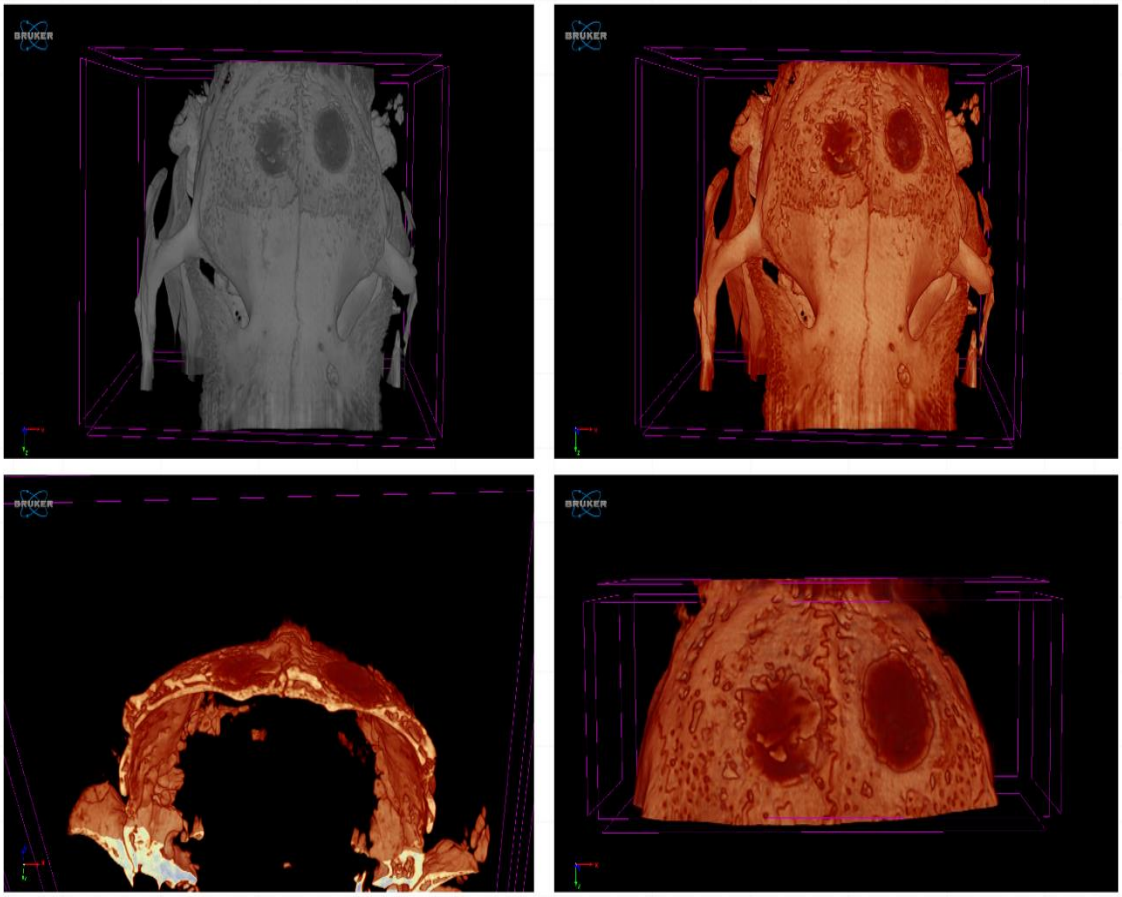

Figure 4.21 CT Images of Non-Cell-Seeded Defect (6L) and Cell-Seeded Defect (6R) in Rabbit 6

Finally, in the sham group, the eighth rabbit (8R and 8L) had 2 critical size defects that were easily observed in the CT images. The average bone volume for the control defects was 0.03 mm^3, indicating no bone regeneration or formation in the absence of the Alg/HAp material. This underscores the necessity of using the Alg/HAp scaffolds for effective bone regeneration.

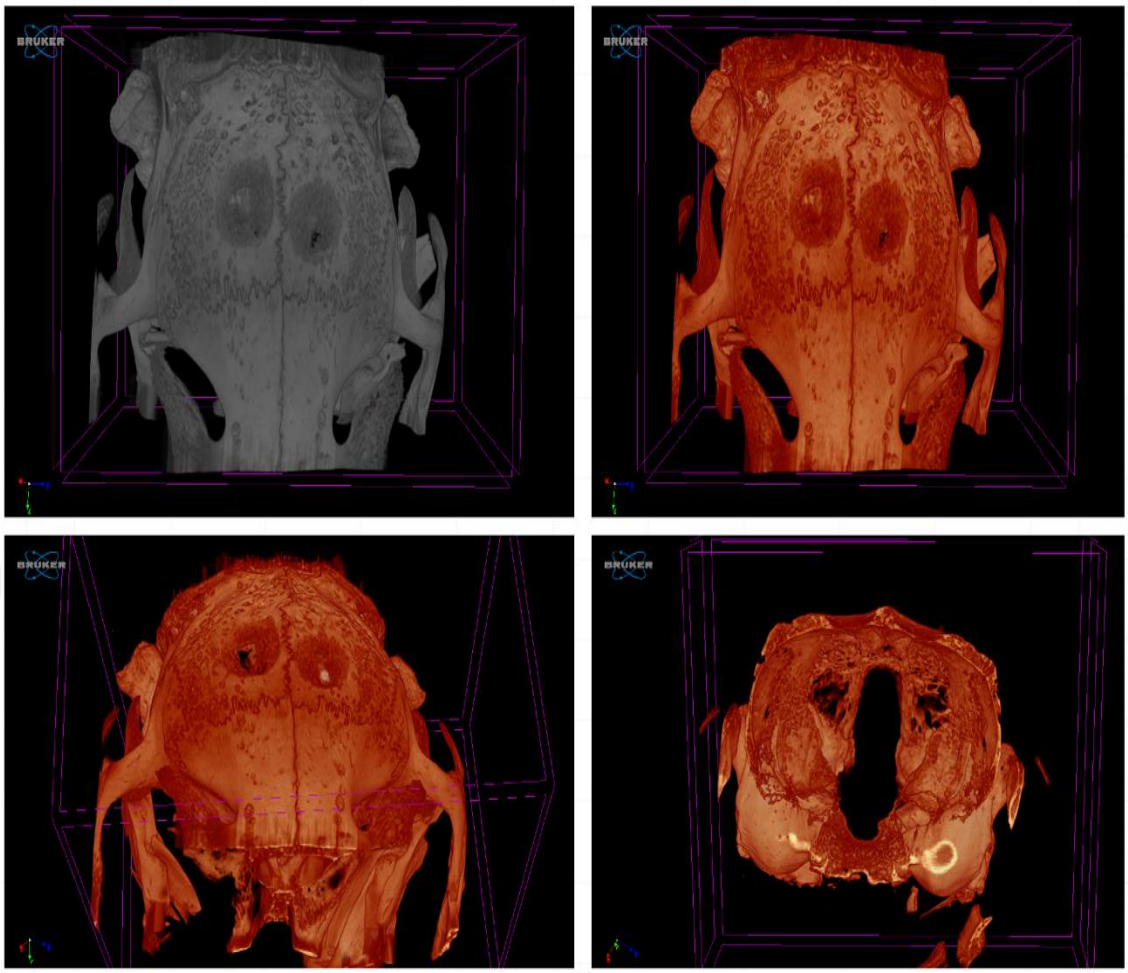

Figure 4.22 CT Images of Control Defects (8R and 8L) in Rabbit 8 (Sham Group)

In **Table 4.5**, it is evident that the cellular group had the highest bone volume and percent bone volume, followed by the acellular group, and lastly, the control group. The bone surface/volume ratio and bone surface density were also higher in the cellular and acellular groups compared to the control, indicating better bone formation and coverage in these groups. The structure model index and trabecular thickness were highest in the cellular group, showing improved structural properties. The trabecular separation and connectivity density were more favorable in the non-cell-seeded group compared to the control group, further emphasizing the effectiveness of the Alg/HAp scaffolds in bone regeneration.

Table 4.5 Average bone volume and structural properties of defects in non-cell-seeded, cell-seeded, and control groups

Description	Format	Unit	Non-cell-seeded	Cell-seeded	Control (sham)
Bone volume	BV	mm^3	27.20 ± 2.27	32.00 ± 0.94	0.03 ± 0.01
Percent bone volume	BV/TV	%	35.30 ± 1.15	38.80 ± 1.39	0.05 ± 0.02
Bone surface / volume ratio	BS/BV	1/mm	7.80 ± 1.87	10.60 ± 0.89	40.60 ± 3.97
Bone surface density	BS/TV	1/mm	2.92 ± 0.84	3.25 ± 0.43	0.02 ± 0.01
Structure model index	SMI		1.27 ± 0.45	2.00 ± 0.53	1.84 ± 0.15
Trabecular thickness	Tb.Th	mm	0.39 ± 0.06	0.56 ± 0.05	0.07 ± 0.02
Trabecular separation	Tb.Sp	mm	2.20 ± 0.08	2.24 ± 0.02	1.02 ± 0.17
Connectivity	Conn		6.10 ± 0.55	10.90 ± 1.27	0.07 ± 0.03
Connectivity density	Conn.Dn	$1/mm^3$	2.40 ± 0.33	2.40 ± 0.23	6.54 ± 0.14

The comparison of average bone volume values across the groups (cell-seeded, non-cell-seeded, and sham group) confirmed that the cell-seeded defects had the highest bone volume, followed by the non-cell-seeded defects, and finally the control defects. Despite the minor differences between the cell-seeded and non-cell-seeded defects, there were several challenges encountered during the *in situ* bioprinting process on some defects, such as crosslinking problems where the stitching process sometimes began before the crosslinking was fully complete, causing the material to disperse within the defect areas. Additionally, bleeding in some defects hindered the *in situ* bioprinting process at times. These factors collectively affected the overall results and bone formation outcomes in some defects but did not diminish the potential of the *in situ* bioprinting of Alg/HAp scaffolds. Hence, these factors need to be addressed in future studies as repeating the study over extended durations to observe long-term outcomes would provide more detailed insights into the efficacy of these scaffolds in bone tissue engineering as well.

5. CONCLUSION

This thesis has explored the potential of *in situ* 3D bioprinting as a transformative approach for craniofacial bone regeneration, addressing the limitations inherent in traditional bone repair methods. Through a comprehensive investigation into the feasibility and effectiveness of this innovative technology, significant strides have been made towards overcoming key challenges associated with bone regeneration and clinical translation.

Traditional methods of treating craniofacial bone defects often involve challenges such as donor site morbidity, the need for multiple surgeries, and insufficient osteogenic properties of the available biomaterials. These conventional approaches are frequently impeded by issues related to donor availability, the complexity and invasiveness of the procedures, and the limited capacity to match the shape and mechanical requirements of the defect site. The advent of 3D bioprinting, however, presents a promising alternative by enabling the precise deposition of cells and biomaterials to create custom scaffolds that can closely mimic the damaged tissue's architecture and functional requirements.

A key achievement of this research is the development of a clinically translatable *in situ* 3D bioprinting strategy for craniofacial bone regeneration. By integrating computer-aided design (CAD) and computer-aided manufacturing (CAM) technologies, this study has demonstrated the capability to model and print scaffolds directly onto damaged tissues, thereby eliminating the traditional two-step process involving in vitro and in vivo experimentation. This methodological advancement not only streamlines the fabrication process but also enhances the practicality of applying this technology in a clinical setting.

The novelty of this study lies in its application of *in situ* bioprinting directly onto the bodies of live animals, as opposed to relying solely on ex vivo or isolated tissue models. This approach ensures a more accurate representation of clinical conditions and potential challenges, thereby improving the relevance and applicability of the findings. By conducting preclinical studies using a rabbit model and employing critical-sized bone

defects on the parietal bones, this research has provided valuable insights into the effectiveness of the proposed bioprinting technique.

The use of Alginate and HAp bioinks in the 3D bioprinting process has proven to be particularly effective. Post-operative evaluations, including CT scans, histopathological analysis, micro-CT imaging, and mechanical testing, revealed successful bone regeneration and integration. These results underscore the potential of the *in situ* bioprinting approach to provide a rapid, patient-specific, and effective regenerative therapy. By directly applying necessary biophysical and biochemical stimuli to the damaged area, this method demonstrates the capacity to significantly enhance bone healing and repair.

In conclusion, this thesis contributes significantly to the growing body of evidence supporting *in situ* 3D bioprinting as a viable and promising technique for craniofacial bone regeneration. The research highlights the potential of this technology to address the limitations of traditional bone repair methods and offers a pathway towards broader clinical applications in tissue engineering and regenerative medicine. The advancements presented here not only pave the way for future research and development in the field but also hold the promise of improving patient outcomes through more effective and personalized regenerative therapies.

The findings of this study provide a solid foundation for further exploration and optimization of *in situ* 3D bioprinting techniques, with the goal of translating these advancements into practical clinical solutions. Future research should focus on refining the technology, expanding its applications, and conducting larger-scale clinical trials to validate and enhance its efficacy. As the field of tissue engineering continues to evolve, the integration of innovative bioprinting strategies will play a crucial role in advancing regenerative medicine and improving the quality of life for patients with craniofacial bone defects and beyond.

REFERENCES

Abdollahiyan, P., Oroojalian, F., Mokhtarzadeh, A., & de la Guardia, M. (2020). Hydrogel-Based 3D Bioprinting for Bone and Cartilage Tissue Engineering. *Biotechnology Journal*, *15*(12). https://doi.org/10.1002/biot.202000095

Abu Owida, H., Al-Ayyad, M., Turab, N. M., & Al-Nabulsi, J. I. (2023). Recent Biomaterial Developments for Bone Tissue Engineering and Potential Clinical Application: Narrative Review of the Literature. *International Journal of Online and Biomedical Engineering (IJOE)*, *19*(15), 4–33. https://doi.org/10.3991/ijoe.v19i15.41879

Agostinacchio, F., Mu, X., Dirè, S., Motta, A., & Kaplan, D. L. (2021). In Situ 3D Printing: Opportunities with Silk Inks. *Trends in Biotechnology*, *39*(7), 719–730. https://doi.org/10.1016/j.tibtech.2020.11.003

Aimar, A., Palermo, A., & Innocenti, B. (2019). The Role of 3D Printing in Medical Applications: A State of the Art. *Journal of Healthcare Engineering*, *2019*, 1–10. https://doi.org/10.1155/2019/5340616

Akilbekova, D., & Mektepbayeva, D. (2017). Patient specific *in situ* 3D printing. In *3D Printing in Medicine* (pp. 91–113). Elsevier. https://doi.org/10.1016/B978-0-08-100717-4.00004-1

Allori, A. C., Sailon, A. M., & Warren, S. M. (2008). Biological Basis of Bone Formation, Remodeling, and Repair—Part I: Biochemical Signaling Molecules. *Tissue Engineering Part B: Reviews*, *14*(3), 259–273. https://doi.org/10.1089/ten.teb.2008.0082

Axpe, E., & Oyen, M. (2016a). Applications of Alginate-Based Bioinks in 3D Bioprinting. *International Journal of Molecular Sciences*, *17*(12), 1976. https://doi.org/10.3390/ijms17121976

Axpe, E., & Oyen, M. (2016b). Applications of Alginate-Based Bioinks in 3D Bioprinting. *International Journal of Molecular Sciences*, *17*(12), 1976. https://doi.org/10.3390/ijms17121976

Badylak, S. F., & Nerem, R. M. (2010). Progress in tissue engineering and regenerative medicine. *Proceedings of the National Academy of Sciences*, *107*(8), 3285–3286. https://doi.org/10.1073/pnas.1000256107

Briquez, P. S., Hubbell, J. A., & Martino, M. M. (2015). Extracellular Matrix-Inspired Growth Factor Delivery Systems for Skin Wound Healing. *Advances in Wound Care*, *4*(8), 479–489. https://doi.org/10.1089/wound.2014.0603

Chen, B., Gao, Q., Song, H., & Xu, M. (2017). Retrospective study of experience of craniofacial reconstruction. *International Wound Journal*, *14*(2), 399–407. https://doi.org/10.1111/iwj.12613

Compaan, A. M., Christensen, K., & Huang, Y. (2017). Inkjet Bioprinting of 3D Silk Fibroin Cellular Constructs Using Sacrificial Alginate. *ACS Biomaterials Science & Engineering*, *3*(8), 1519–1526. https://doi.org/10.1021/acsbiomaterials.6b00432

Cui, X., Li, J., Hartanto, Y., Durham, M., Tang, J., Zhang, H., Hooper, G., Lim, K., & Woodfield, T. (2020). Advances in Extrusion 3D Bioprinting: A Focus on Multicomponent Hydrogel-Based Bioinks. *Advanced Healthcare Materials*, *9*(15). https://doi.org/10.1002/adhm.201901648

Dawood, A., Marti, B. M., Sauret-Jackson, V., & Darwood, A. (2015). 3D printing in dentistry. *British Dental Journal*, *219*(11), 521–529. https://doi.org/10.1038/sj.bdj.2015.914

Derby, B. (2012). Printing and Prototyping of Tissues and Scaffolds. *Science*, *338*(6109), 921–926. https://doi.org/10.1126/science.1226340

Dhandayuthapani, B., Yoshida, Y., Maekawa, T., & Kumar, D. S. (2011). Polymeric Scaffolds in Tissue Engineering Application: A Review. *International Journal of Polymer Science*, *2011*, 1–19. https://doi.org/10.1155/2011/290602

Di Bella, C., Duchi, S., O'Connell, C. D., Blanchard, R., Augustine, C., Yue, Z., Thompson, F., Richards, C., Beirne, S., Onofrillo, C., Bauquier, S. H., Ryan, S. D., Pivonka, P., Wallace, G. G., & Choong, P. F. (2018). *In situ* handheld three-dimensional bioprinting for cartilage regeneration. *Journal of Tissue Engineering and Regenerative Medicine*, *12*(3), 611–621. https://doi.org/10.1002/term.2476

Dzobo, K., Motaung, K. S. C. M., & Adesida, A. (2019). Recent Trends in Decellularized Extracellular Matrix Bioinks for 3D Printing: An Updated Review. *International Journal of Molecular Sciences*, *20*(18), 4628. https://doi.org/10.3390/ijms20184628

Emara, A., & Shah, R. (2021). Recent update on craniofacial tissue engineering. *Journal of Tissue Engineering*, *12*, 204173142110037. https://doi.org/10.1177/20417314211003735

Farshidfar, N., Iravani, S., & Varma, R. S. (2023). Alginate-Based Biomaterials in Tissue Engineering and Regenerative Medicine. *Marine Drugs*, *21*(3), 189. https://doi.org/10.3390/md21030189

Fatimi, A., Okoro, O. V., Podstawczyk, D., Siminska-Stanny, J., & Shavandi, A. (2022). Natural Hydrogel-Based Bio-Inks for 3D Bioprinting in Tissue Engineering: A Review. *Gels*, *8*(3), 179. https://doi.org/10.3390/gels8030179

Feng, Y., Guo, W., Hu, L., Yi, X., & Tang, F. (2022). Application of Hydrogels as Sustained-Release Drug Carriers in Bone Defect Repair. *Polymers*, *14*(22), 4906. https://doi.org/10.3390/polym14224906

Freyman, T. M., Yannas, I. V., & Gibson, L. J. (2001). Cellular materials as porous scaffolds for tissue engineering. *Progress in Materials Science*, *46*(3–4), 273–282. https://doi.org/10.1016/S0079-6425(00)00018-9

Furth, M. E., & Atala, A. (2014). Tissue Engineering. In *Principles of Tissue Engineering* (pp. 83–123). Elsevier. https://doi.org/10.1016/B978-0-12-398358-9.00006-9

Gazit, Z., Pelled, G., Sheyn, D., Yakubovich, D. C., & Gazit, D. (2019). Mesenchymal Stem Cells. In *Principles of Regenerative Medicine* (pp. 205–218). Elsevier. https://doi.org/10.1016/B978-0-12-809880-6.00014-X

Gu, Z., Fu, J., Lin, H., & He, Y. (2020). Development of 3D bioprinting: From printing methods to biomedical applications. *Asian Journal of Pharmaceutical Sciences*, *15*(5), 529–557. https://doi.org/10.1016/j.ajps.2019.11.003

Hasirci V., Y. D. (2007). *Hasirci V., Yucel D. Polymers Used in Tissue Engineering, in Encyclopedia of Biomaterials and Biomedical Engineering 2007, 1:1, 1-17.*

Heid, S., & Boccaccini, A. R. (2020). Advancing bioinks for 3D bioprinting using reactive fillers: A review. *Acta Biomaterialia*, *113*, 1–22. https://doi.org/10.1016/j.actbio.2020.06.040

Huri, P. Y., Hamsici, S., Ergene, E., Huri, G., & Doral, M. N. (2018). Infrapatellar Fat Pad-Derived Stem Cell-Based Regenerative Strategies in Orthopedic Surgery. *Knee Surgery and Related Research*, *30*(3), 179–186. https://doi.org/10.5792/ksrr.17.061

Iglesias-Mejuto, A., & García-González, C. A. (2021). 3D-printed alginate-hydroxyapatite aerogel scaffolds for bone tissue engineering. *Materials Science and Engineering: C*, *131*, 112525. https://doi.org/10.1016/j.msec.2021.112525

Jakus, A. E., Rutz, A. L., & Shah, R. N. (2016). Advancing the field of 3D biomaterial printing. *Biomedical Materials*, *11*(1), 014102. https://doi.org/10.1088/1748-6041/11/1/014102

Jovic, T. H., Kungwengwe, G., Mills, A. C., & Whitaker, I. S. (2019). Plant-Derived Biomaterials: A Review of 3D Bioprinting and Biomedical Applications. *Frontiers in Mechanical Engineering*, *5*. https://doi.org/10.3389/fmech.2019.00019

Kellomäki, M., Niiranen, H., Puumanen, K., Ashammakhi, N., Waris, T., & Törmälä, P. (2000). Bioabsorbable scaffolds for guided bone regeneration and generation. *Biomaterials*, *21*(24), 2495–2505. https://doi.org/10.1016/S0142-9612(00)00117-4

Khademhosseini, A., & Langer, R. (2016). A decade of progress in tissue engineering. *Nature Protocols*, *11*(10), 1775–1781. https://doi.org/10.1038/nprot.2016.123

Kim, H. T., Teng, M. S., & Dang, A. C. (2008). Chondrocyte Apoptosis: Implications for Osteochondral Allograft Transplantation. *Clinical Orthopaedics and Related Research*, *466*(8), 1819–1825. https://doi.org/10.1007/s11999-008-0304-6

Klebe, R. J. (1988). Cytoscribing: A method for micropositioning cells and the construction of two- and three-dimensional synthetic tissues. *Experimental Cell Research*, *179*(2), 362–373. https://doi.org/10.1016/0014-4827(88)90275-3

Kruijt Spanjer, E. C., Bittermann, G. K. P., van Hooijdonk, I. E. M., Rosenberg, A. J. W. P., & Gawlitta, D. (2017). Taking the endochondral route to craniomaxillofacial bone regeneration: A logical approach? *Journal of Cranio-Maxillofacial Surgery*, *45*(7), 1099–1106. https://doi.org/10.1016/j.jcms.2017.03.025

Landers, R., Hübner, U., Schmelzeisen, R., & Mülhaupt, R. (2002). Rapid prototyping of scaffolds derived from thermoreversible hydrogels and tailored for applications in tissue engineering. *Biomaterials*, *23*(23), 4437–4447. https://doi.org/10.1016/S0142-9612(02)00139-4

Landers, R., & Mülhaupt, R. (2000). Desktop manufacturing of complex objects, prototypes and biomedical scaffolds by means of computer-assisted design combined with computer-guided 3D plotting of polymers and reactive oligomers. *Macromolecular Materials and Engineering*, *282*(1), 17–21. https://doi.org/10.1002/1439-2054(20001001)282:1<17::AID-MAME17>3.0.CO;2-8

Lee, J., Hong, J., Kim, W., & Kim, G. H. (2020). Bone-derived dECM/alginate bioink for fabricating a 3D cell-laden mesh structure for bone tissue engineering. *Carbohydrate Polymers*, *250*, 116914. https://doi.org/10.1016/j.carbpol.2020.116914

Li, L., Shi, J., Ma, K., Jin, J., Wang, P., Liang, H., Cao, Y., Wang, X., & Jiang, Q. (2021). Robotic *in situ* 3D bio-printing technology for repairing large segmental bone defects. *Journal of Advanced Research*, *30*, 75–84. https://doi.org/10.1016/j.jare.2020.11.011

Li, L., Yu, F., Shi, J., Shen, S., Teng, H., Yang, J., Wang, X., & Jiang, Q. (2017a). In situ repair of bone and cartilage defects using 3D scanning and 3D printing. *Scientific Reports*, *7*(1). https://doi.org/10.1038/s41598-017-10060-3

Li, L., Yu, F., Shi, J., Shen, S., Teng, H., Yang, J., Wang, X., & Jiang, Q. (2017b). In situ repair of bone and cartilage defects using 3D scanning and 3D printing. *Scientific Reports*, *7*(1), 9416. https://doi.org/10.1038/s41598-017-10060-3

Lima, T. de P. L., Canelas, C. A. d. A., Concha, V. O. C., Costa, F. A. M. da, & Passos, M. F. (2022). 3D Bioprinting Technology and Hydrogels Used in the Process. *Journal of Functional Biomaterials*, *13*(4), 214. https://doi.org/10.3390/jfb13040214

Lipskas, J., Deep, K., & Yao, W. (2019). Robotic-Assisted 3D Bio-printing for Repairing Bone and Cartilage Defects through a Minimally Invasive Approach. *Scientific Reports*, *9*(1), 3746. https://doi.org/10.1038/s41598-019-38972-2

Liu, L., Zhang, L., Ren, B., Wang, F., & Zhang, Q. (2003). Preparation and Characterization of Collagen–Hydroxyapatite Composite Used for Bone Tissue Engineering Scaffold. *Artificial Cells, Blood Substitutes, and Biotechnology*, *31*(4), 435–448. https://doi.org/10.1081/BIO-120025414

Luo, Y., Tan, J., Zhou, Y., Guo, Y., Liao, X., He, L., Li, D., Li, X., & Liu, Y. (2023). From crosslinking strategies to biomedical applications of hyaluronic acid-based hydrogels: A review. *International Journal of Biological Macromolecules*, *231*, 123308. https://doi.org/10.1016/j.ijbiomac.2023.123308

Ma, K., Zhao, T., Yang, L., Wang, P., Jin, J., Teng, H., Xia, D., Zhu, L., Li, L., Jiang, Q., & Wang, X. (2020). Application of robotic-assisted *in situ* 3D printing in cartilage regeneration with HAMA hydrogel: An in vivo study. *Journal of Advanced Research*, *23*, 123–132. https://doi.org/10.1016/j.jare.2020.01.010

Malafaya, P. B., Silva, G. A., & Reis, R. L. (2007). Natural–origin polymers as carriers and scaffolds for biomolecules and cell delivery in tissue engineering applications. *Advanced Drug Delivery Reviews*, *59*(4–5), 207–233. https://doi.org/10.1016/j.addr.2007.03.012

Malikmammadov, E., Tanir, T. E., Kiziltay, A., Hasirci, V., & Hasirci, N. (2018). PCL and PCL-based materials in biomedical applications. *Journal of Biomaterials Science, Polymer Edition*, *29*(7–9), 863–893. https://doi.org/10.1080/09205063.2017.1394711

Mertz, L. (2017). Tissue Engineering and Regenerative Medicine: The Promise, the Challenges, the Future. *IEEE Pulse*, *8*(3), 15–18. https://doi.org/10.1109/MPUL.2017.2678101

Mikos, A. G., Sarakinos, G., Leite, S. M., Vacant, J. P., & Langer, R. (1993). Laminated three-dimensional biodegradable foams for use in tissue engineering. *Biomaterials*, *14*(5), 323–330. https://doi.org/10.1016/0142-9612(93)90049-8

Moreno Madrid, A. P., Vrech, S. M., Sanchez, M. A., & Rodriguez, A. P. (2019). Advances in additive manufacturing for bone tissue engineering scaffolds. *Materials Science and Engineering: C*, *100*, 631–644. https://doi.org/10.1016/j.msec.2019.03.037

Muhamad, I. I., Selvakumaran, S., & Lazim, N. A. (2014). Designing Polymeric Nanoparticles for Targeted Drug Delivery System. In Professor Alexander Seifalian, Achala de Mel, & Deepak M. Kalaskar (Eds.), Nanomedicine. One Central Press (OCP). (n.d.).

Murdock, M. H., & Badylak, S. F. (2017). Biomaterials-based *in situ* tissue engineering. *Current Opinion in Biomedical Engineering*, *1*, 4–7. https://doi.org/10.1016/j.cobme.2017.01.001

Murphy, S. V, & Atala, A. (2014). 3D bioprinting of tissues and organs. *Nature Biotechnology*, *32*(8), 773–785. https://doi.org/10.1038/nbt.2958

Naghieh, S., & Chen, X. (2021). Printability–A key issue in extrusion-based bioprinting. *Journal of Pharmaceutical Analysis*, *11*(5), 564–579. https://doi.org/10.1016/j.jpha.2021.02.001

Norotte, C., Marga, F. S., Niklason, L. E., & Forgacs, G. (2009). Scaffold-free vascular tissue engineering using bioprinting. *Biomaterials*, *30*(30), 5910–5917. https://doi.org/10.1016/j.biomaterials.2009.06.034

Nulty, J., Freeman, F. E., Browe, D. C., Burdis, R., Ahern, D. P., Pitacco, P., Lee, Y. Bin, Alsberg, E., & Kelly, D. J. (2021). 3D bioprinting of prevascularised implants for the repair of critically-sized bone defects. *Acta Biomaterialia*, *126*, 154–169. https://doi.org/10.1016/j.actbio.2021.03.003

Odde, D. J., & Renn, M. J. (1999). Laser-guided direct writing for applications in biotechnology. *Trends in Biotechnology*, *17*(10), 385–389. https://doi.org/10.1016/S0167-7799(99)01355-4

Ozbolat, I. T., & Hospodiuk, M. (2016). Current advances and future perspectives in extrusion-based bioprinting. *Biomaterials*, *76*, 321–343. https://doi.org/10.1016/J.BIOMATERIALS.2015.10.076

Ozbolat, I. T., Moncal, K. K., & Gudapati, H. (2017). Evaluation of bioprinter technologies. *Additive Manufacturing*, *13*, 179–200. https://doi.org/10.1016/J.ADDMA.2016.10.003

Panwar, A., & Tan, L. (2016). Current Status of Bioinks for Micro-Extrusion-Based 3D Bioprinting. *Molecules*, *21*(6), 685. https://doi.org/10.3390/molecules21060685

Peterson, B., Whang, P. G., Iglesias, R., Wang, J. C., & Lieberman, J. R. (2004). Osteoinductivity of Commercially Available Demineralized Bone Matrix. *The Journal of Bone & Joint Surgery*, *86*(10), 2243–2250. https://doi.org/10.2106/00004623-200410000-00016

Qu, H., Fu, H., Han, Z., & Sun, Y. (2019). Biomaterials for bone tissue engineering scaffolds: a review. *RSC Advances*, *9*(45), 26252–26262. https://doi.org/10.1039/C9RA05214C

Ramasamy, S., Davoodi, P., Vijayavenkataraman, S., Teoh, J. H., Thamizhchelvan, A. M., Robinson, K. S., Wu, B., Fuh, J. Y. H., DiColandrea, T., Zhao, H., Lane, E. B., & Wang, C.-H. (2021). Optimized construction of a full thickness human skin equivalent using 3D bioprinting and a PCL/collagen dermal scaffold. *Bioprinting*, *21*, e00123. https://doi.org/10.1016/j.bprint.2020.e00123

Reddi, A. H., & Reddi, A. (2009). Bone morphogenetic proteins (BMPs): From morphogens to metabologens. *Cytokine & Growth Factor Reviews*, *20*(5–6), 341–342. https://doi.org/10.1016/j.cytogfr.2009.10.015

Sánchez-Salazar, M. G., Álvarez, M. M., & Trujillo-de Santiago, G. (2021). Advances in 3D bioprinting for the biofabrication of tumor models. *Bioprinting*, *21*, e00120. https://doi.org/10.1016/j.bprint.2020.e00120

Saygili, E., Dogan-Gurbuz, A. A., Yesil-Celiktas, O., & Draz, M. S. (2020). 3D bioprinting: A powerful tool to leverage tissue engineering and microbial systems. *Bioprinting*, *18*, e00071. https://doi.org/10.1016/J.BPRINT.2019.E00071

Schott, N. G., Friend, N. E., & Stegemann, J. P. (2021). Coupling Osteogenesis and Vasculogenesis in Engineered Orthopedic Tissues. *Tissue Engineering Part B: Reviews*, *27*(3), 199–214. https://doi.org/10.1089/ten.teb.2020.0132

Shafiee, A., & Atala, A. (2017). Tissue Engineering: Toward a New Era of Medicine. *Annual Review of Medicine*, *68*(1), 29–40. https://doi.org/10.1146/annurev-med-102715-092331

Skardal, A., Mack, D., Kapetanovic, E., Atala, A., Jackson, J. D., Yoo, J., & Soker, S. (2012). Bioprinted Amniotic Fluid-Derived Stem Cells Accelerate Healing of Large Skin Wounds. *Stem Cells Translational Medicine*, *1*(11), 792–802. https://doi.org/10.5966/sctm.2012-0088

Spencer, E. M., Liu, C. C., Si, E. C. C., & Howard, G. A. (1991). In vivo actions of insulin-like growth factor-I (IGF-I) on bone formation and resorption in rats. *Bone*, *12*(1), 21–26. https://doi.org/10.1016/8756-3282(91)90050-S

Su, X., Si, X., Liu, Y., Xiong, N., Li, S., Tang, L., Shi, Z., Cheng, L., & Zhang, F. (2024). Comparison of different hydroxyapatite composites for bone tissue repair: In vitro and in vivo analyses. *Iranian Journal of Basic Medical Sciences*, *27*(9), 1155–1161. https://doi.org/10.22038/IJBMS.2024.78578.16995

Suo, H., Chen, Y., Liu, J., Wang, L., & Xu, M. (2021). 3D printing of biphasic osteochondral scaffold with sintered hydroxyapatite and polycaprolactone. *Journal of Materials Science*, *56*(29), 16623–16633. https://doi.org/10.1007/s10853-021-06229-x

Sutherland, D., & Bostrom, M. (2005). Grafts and Bone Graft Substitutes. In *Bone Regeneration and Repair* (pp. 133–156). Humana Press. https://doi.org/10.1385/1-59259-863-3:133

Ventura, R. D. (2021). An Overview of Laser-assisted Bioprinting (LAB) in Tissue Engineering Applications. *Medical Lasers*, *10*(2), 76–81. https://doi.org/10.25289/ML.2021.10.2.76

Villa, M. M., Wang, L., Huang, J., Rowe, D. W., & Wei, M. (2015). Bone tissue engineering with a collagen-hydroxyapatite scaffold and culture expanded bone marrow stromal cells. *Journal of Biomedical Materials Research Part B: Applied Biomaterials*, *103*(2), 243–253. https://doi.org/10.1002/jbm.b.33225

Wilson, W. C., & Boland, T. (2003). Cell and organ printing 1: Protein and cell printers. *The Anatomical Record Part A: Discoveries in Molecular, Cellular, and Evolutionary Biology*, *272A*(2), 491–496. https://doi.org/10.1002/ar.a.10057

Wu, Y., Lin, Z. Y. (William), Wenger, A. C., Tam, K. C., & Tang, X. (Shirley). (2018). 3D bioprinting of liver-mimetic construct with alginate/cellulose nanocrystal hybrid bioink. *Bioprinting*, *9*, 1–6. https://doi.org/10.1016/j.bprint.2017.12.001

Yang, J., Zhang, Y. S., Yue, K., & Khademhosseini, A. (2017). Cell-laden hydrogels for osteochondral and cartilage tissue engineering. *Acta Biomaterialia*, *57*, 1–25. https://doi.org/10.1016/j.actbio.2017.01.036

Younger, E. M., & Chapman, M. W. (1989). Morbidity at Bone Graft Donor Sites. *Journal of Orthopaedic Trauma*, *3*(3), 192–195. https://doi.org/10.1097/00005131-198909000-00002

Zhang, Y., Kumar, P., Lv, S., Xiong, D., Zhao, H., Cai, Z., & Zhao, X. (2021). Recent advances in 3D bioprinting of vascularized tissues. *Materials & Design*, *199*, 109398. https://doi.org/10.1016/j.matdes.2020.109398

Zhou, Y., Qin, R., Chen, T., Zhang, K., & Gui, J. (2021). 3D bioprinting modified autologous matrix-induced chondrogenesis(AMIC) technique for repair of cartilage defects. *Materials & Design*, *203*, 109621. https://doi.org/10.1016/j.matdes.2021.109621